MASTERARBEIT

Rückkopplungsanalyse in Klimaänderungssimulationen

Feedback analysis of climate change simulations

Vanessa Simone Rieger

Betreuung:
Prof. Dr. Bernhard Mayer
Dr. Michael Ponater

Ludwig-Maximilians-Universität München
Fakultät für Physik

Deutsches Zentrum für Luft- und Raumfahrt

München, Juni 2014

Abstract

The climate sensitivity parameter that describes the change in surface temperature due to a unit change in radiative forcing has long been assumed to be constant. However, recent studies found that the climate sensitivity parameter varies, not only amongst models for the same forcing but also within the same model where it may strongly depend on the strength and on the type of the applied radiative forcing.

By means of the "Partial Radiative Perturbation"-method (PRP-method), a complete feedback analysis of CO_2 driven climate change simulations is performed to identify the individual feedback processes which are responsible for the variation in climate sensitivity parameter. To include all components of the feedback analysis, the stratospheric temperature feedback is introduced in this work. It describes the stratospheric temperature change due to a radiative forcing. This feedback is found to be weakly positive. The combination of the stratospheric temperature feedback and the instantaneous radiative forcing allows to approximate the stratosphere adjusted radiative forcing which is known to be a better climate predictor than the instantaneous forcing.

In a set of CO_2 driven equilibrium climate change simulations, the water vapour, the cloud and the stratospheric temperature feedback are found to vary the most under increasing radiative forcing. Hence, the interplay between these three feedback processes causes an increase of the climate sensitivity parameter when the atmospheric carbon dioxide concentration is quadrupled in comparison to a doubling of the CO_2 concentration. For climate change simulations with a small CO_2 radiative forcing, it was not possible to identify the feedback processes which are responsible for a varying climate sensitivity parameter. Thus, forcings must be sufficiently large to establish significant differences of feedbacks that are interpretable to explain differences in climate sensitivities.

Feedbacks of CO_2 driven simulations with and without interactively coupled atmospheric chemistry are also compared. Only the stratospheric temperature feedback differs significantly among these simulation experiments. For the simulation without interactively coupled chemistry, the stratospheric temperature feedback is considerably larger than for the simulation with interactively coupled chemistry where the trace gases could adjust to the radiative perturbation. The change in ozone is found to be responsible for the difference between these simulations. Ozone changes to a CO_2 radiative forcing causes a negative feedback, which reduces the stratospheric temperature feedback, when the reaction of the atmospheric chemistry to the CO_2 perturbation is included.

Moreover, the strengths and weaknesses of the PRP-method are investigated. This method is only suitable for calculating independent feedbacks and to yield a balance of radiative forcing and feedbacks, if the forward and backward PRP calculations are combined. If only the forward or the backward PRP calculation is considered, interactions between feedbacks occur, which render the separation of the climate response into individual feedbacks as unpracticable. In particular, the water vapour and the lapse rate feedback as well as the water vapour and the cloud feedback show large overlapping effects. These overlapping effects are completely erased when forward and backward PRP calculations are combined.

Contents

1 Introduction **1**

2 Theoretical background **4**
2.1 Radiation balance of the Earth 4
2.2 Radiative forcing and climate sensitivity 6
2.3 Climate feedbacks 7

3 Feedback analysis method and model description **11**
3.1 "Partial Radiative Perturbation"-Method 11
3.2 Model and simulation set-up 12
3.3 Separation of feedback processes 14

4 Results **15**
4.1 Climate feedbacks of CO_2 doubling simulation 15
4.2 Temporal variability of climate feedbacks 19
4.3 Comparison of feedbacks between simulations with and without interactively coupled atmospheric chemistry 21
4.4 Additivity of climate feedbacks 22
4.5 Climate feedbacks under selected CO_2 driven climate change simulations . 26

5 Discussion **32**

A Appendix **38**
A.1 Input parameters for CO_2 doubling experiment 38
A.2 Supplementary results of CO_2 doubling experiment 39
A.3 Results of 442CO2 simulation 42
A.4 Results of 4xCO2 simulation 44

1 Introduction

Human influence on the climate is evident. Since the industrialisation in the 18th century, the atmospheric concentration of carbon dioxide has raised to levels which are unprecedented in the last 800,000 years. Other anthropogenic emissions have also increased significantly since the begin of the industrial era. The Fifth Assessment Report (AR5) of the Intergovernmental Panel on Climate Change (IPCC) reports that human impacts on the climate system are extremely likely the main reason for the global warming observed since the 1950s. In 2011, the carbon dioxide concentration had reached a value of 391 ppm which is by about 40% higher than the pre-industrial level. Further, ice cores records show that the rate of CO_2 increase over the past century is the highest in the last 22,000 years. Mainly emissions from fossil fuel burning and land use changes are responsible for this strong increase. (IPCC, 2013)

In the 19th century, observations and instrumental detection of climate variables began. Together with paleoclimate reconstructions, climate's development can be traced back hundreds to millions of years. Since the mid-20th century, the warming of the climate cannot be dismissed. The global surface temperature over land and ocean increased by 0.85 (0.65 to 1.06) K from 1880 to 2012. Moreover, observations show that snow and ice masses have reduced significantly, while the sea level rose by 0.19 m in the last century. (IPCC, 2013)

Appropriate interplay of observations and model simulations of temperature change, climate feedbacks, and modifications in the Earth's energy budget enables to validate and to project future climates. Nevertheless, the forecast of future climate has remained uncertain. Fig. 1.1 presents the modelled evolution of the global mean surface temperature up to the year 2100 for different emission scenarios. The global warming, determined by the mean surface temperature rise of each scenarios, ranges from 1.0 to 3.7 K when averaged over the last 20 years of the 22th century. However, even for one particular emission scenario, the uncertainty of the projected temperature development is large. For example, for the RCP8.5 scenario, where the CO_2 concentration increases continuously to a value of 936 ppm in 2100, the surface temperature increase ranges from 2.6 to 4.8 K. To narrow the modelled uncertainty of climate projections, it is essential to improve our understanding of climate processes.

Feedback analyses are an important prerequisite to comprehend the processes of future climate development (Bony et al., 2006). Many studies have already investigated climate feedbacks. From the global perspective (i.e. the global mean temperature change, as displayed in Fig. 1.1), it is most important to calculate, understand, and verify global mean radiative feedbacks. These are, however, a result of a large number of regional and local physical processes. To determine the parts of the Earth's surface and of the atmosphere which contributes the most to the feedback processes, the geographical and

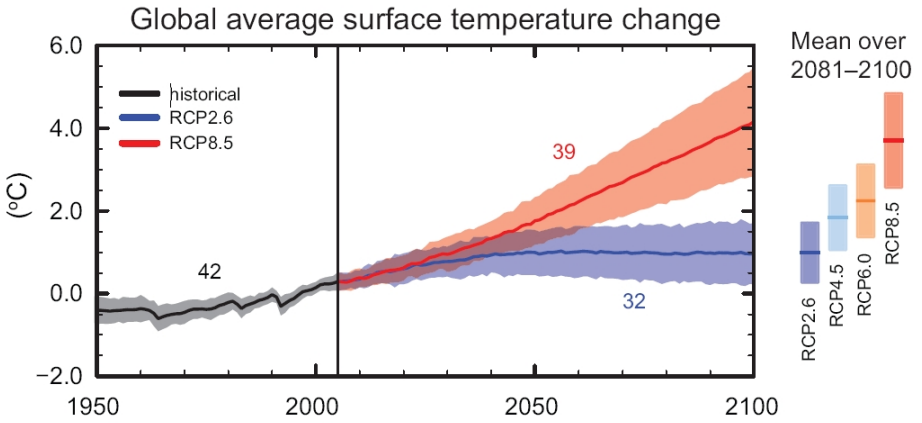

Figure 1.1: Multi-model projections of global mean surface temperature change from 1950 to 2100 relative to 1986-2005 due to various emission scenarios. The black line presents the modelled historical evolution. Shaded areas indicate the uncertainties. The numbers of used models are displayed. (IPCC, 2013)

vertical distributions were examined by Colman (2001, 2002). Soden and Held (2006) compared the main physical climate feedbacks such as temperature, water vapour, albedo, and cloud feedback for different general circulation models. In particular, the cloud feedback shows a large spread among different models. Already 25 years ago, Cess et al. (1990) concluded that this high model to model variability of the cloud feedback is the main source of uncertainty in atmospheric general circulation models. To further investigate the cloud feedback, Colman et al. (2001) split up the cloud feedback into components due to cloud amount, cloud height, water content, water phase, physical thickness and convective cloud fraction and also examined the cloud impact on other feedbacks. So far, the validation of the global mean cloud feedback with observations is not possible since globalwide observations of all relevant cloud parameters are not available. Although progress in understanding feedback processes has been made in the last years (Bony et al., 2006), there are still many open questions.

The intermodel variability of climate predictions is best illustrated by the *climate sensitivity parameter*, which describes the ratio of the global mean surface temperature change and the applied external perturbation. Depending on model physics and model resolutions, the climate sensitivity parameters may vary. However, also the strength and the nature of the forcing influence this parameter (Hansen et al., 2005). One of the few models of the world for which a decade of research concerning climate sensitivity is available is the ECHAM climate model (e.g. Roeckner et al., 1999; Stuber et al., 2005; Ponater et al., 2012). Recently, it has been developed towards the EMAC global chemistry climate model (Joeckel et al., 2006; Sausen et al., 2010; Dietmüller, 2011). The climate sensitivity of EMAC is found to be in good agreement to other climate models (Soden and Held, 2006). Furthermore, Dietmüller (2011) reports that the climate sensitivity

parameter of EMAC varies under different strength and different type of perturbations. She performed several carbon dioxide driven simulations where the atmospheric CO_2 concentration was (a) increased by 75 ppmv to a level of 442 ppmv, (b) doubled to a level of 734 ppmv, and (c) quadrupled to 1468 ppmv. Dietmüller et al. (2014) assessed that the climate does not respond linearly to the applied perturbation. For the simulation with the quadrupled CO_2 concentration, the climate sensitivity parameter increases by about 30% when compared to the doubled CO_2 simulation. The topic of this thesis is to identify the feedback processes which are responsible for this increase of climate sensitivity. Therefore, a complete feedback analysis is performed.

Chapter 2 introduces the theoretical background with the respective concepts of radiative forcing, climate sensitivity, and climate feedbacks as mentioned above. Chapter 3 describes the "Partial Radiative Perturbation"-method and the radiative transfer model which forms the basis to analyse the feedbacks. Results are presented and discussed in Chapter 4. The global distribution of feedbacks as well as the global mean value of the shortwave and longwave components of the Planck feedback, lapse rate feedback, stratospheric temperature feedback (a term introduced in this work), albedo feedback, water vapour feedback and cloud feedback for the standard case of a doubling of the atmospheric CO_2 concentration are presented and their temporal variability are investigated. Dietmüller (2011) performed further simulations with and without interactively coupled atmospheric chemistry which shall be compared in Chapter 4.3. The additivity of feedback processes is examined in Chapter 4.4. The feedbacks of the three CO_2 driven simulation experiments are compared to each other to be able to address possible reasons of a varying climate sensitivity in Chapter 4.5. Finally, the results are discussed in Chapter 5, including some conclusions as well as recommendations for further work.

2 Theoretical background

2.1 Radiation balance of the Earth

The global energy balance of incoming solar (shortwave) radiation and outgoing terrestrial (longwave) radiation determines Earth's climate (Fig. 2.1). The sun heats the Earth and thus increases Earth's temperature until it is compensated by the thermal longwave radiation.

Each body which has a temperature higher than absolute zero acts as a grey body and emits longwave radiation back to its surroundings. The *Stefan-Boltzmann law* describes the relationship of the total emitted radiation energy F per unit surface area and time of such a grey body and its temperature T:

$$F = \epsilon \, \sigma \, T^4 \tag{2.1}$$

with σ being the *Stefan-Boltzmann constant*. For a black body which completely absorbs the received radiation, the emissivity ϵ has a value of 1. However, the Earth acts a grey body as it does not completely absorb incoming radiation but also scatters part of it back to space. The integrated emissivity of the Earth's surface has a value of 0.95. (see review of Ponater et al., 2012)

Following the Stefan-Boltzmann law (Eq. 2.1), the Earth emits the absorbed solar energy as terrestrial radiation back to space and thus balances the incoming solar insolation. The radiation balance of the Earth is further strongly influenced by the Earth's atmosphere. The atmosphere contains several gases such as water vapour, carbon dioxide, ozone, methane, and nitrous dioxide which are substantially radiatively active in the longwave spectral range. These so-called greenhouse gases absorb and re-emit the terrestrial radiation received from the Earth's surface, which in turn rises the surface temperature. This mechanism is called the atmospheric *greenhouse effect*. It increases the Earth's surface temperature by 30 K. Without an atmosphere, the global mean surface temperature of the Earth would be only -15 °C. The most important greenhouse gas is the water vapour followed by the carbon dioxide. (see review of Ponater et al., 2012)

The solar radiation spectrum ranges roughly from wavelength 0.2 to 3.5 μm whereas the terrestrial radiation spectrum stretches from about wavelength 3.5 to 100 μm. Little overlap occurs between the two spectral ranges and hence for practical purposes, they can be treated separately as it is also indicated in Fig. 2.1. (Zdunkowski et al., 2007)

To quantify radiation transfer in the atmosphere, *radiation fluxes* are used. Radiation flux (given in Wm^{-2}) describes the total energy of the radiation passing through or hitting a surface per unit time and per unit area. Basic physics imply that absorption

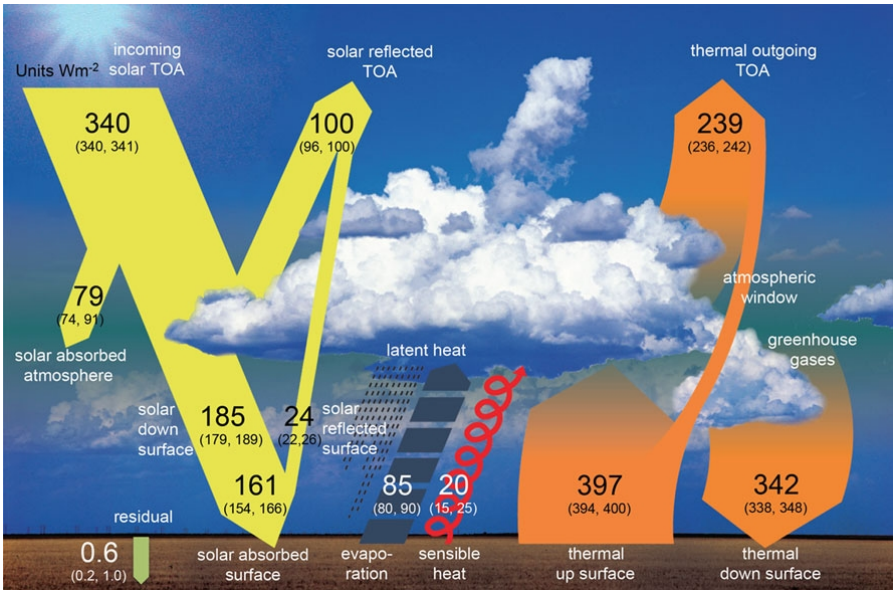

Figure 2.1: Schematic figure of the global mean energy budget of the Earth (Wild et al., 2013)

and emission of gases are extremely wavelength dependent, and thus described by a spectrally dependent quantity, the spectral irradiance F_λ. To obtain the flux F of a wavelength interval, the spectral flux F_λ needs to be integrated over the interval range $[\lambda_1, \lambda_2]$ as follows:

$$F(\lambda_1, \lambda_2) = \int_{\lambda_1}^{\lambda_2} F_\lambda \, d\lambda \tag{2.2}$$

The shortwave radiation flux is calculated by integrating over the shortwave spectral range, the longwave flux over the longwave spectral range, respectively. (Petty, 2006)

To determine the shortwave and longwave radiation fluxes in the atmosphere, the atmosphere is divided into several horizontal layers. At each boundary layer, fluxes pointing *upward* and *downward* occur. The upward flux is calculated by integrating the intensity I over all possible directions pointing skyward. The intensity indicates the strength of a flux per unit solid angle. By regarding spherical polar coordinates with the z-axis being perpendicular to the surface, the upward flux is calculated as follows:

$$F^{\uparrow} = -\int_0^{2\pi} \int_0^{\pi/2} I(\theta, \phi) \cos\theta \, \sin\theta \, d\theta d\phi \tag{2.3}$$

Equivalently, the downward flux is determined:

$$F^{\downarrow} = -\int_0^{2\pi} \int_{\pi/2}^{\pi} I(\theta, \phi) \cos\theta \, \sin\theta \, d\theta d\phi \tag{2.4}$$

Upward and downward fluxes are defined in such a way that the upward-directed fluxes have a negative sign and downward-directed fluxes a positive sign. The sum of the upward and downward fluxes is defined as the *net flux*:

$$F^{net} = F^{\uparrow} + F^{\downarrow} \tag{2.5}$$

These calculation steps to determine the upward, downward, and net fluxes are performed for the corresponding spectral bands of the solar and terrestrial spectral ranges to quantify the shortwave and longwave fluxes in the atmosphere. (Petty, 2006)

2.2 Radiative forcing and climate sensitivity

The energy balance of the solar and terrestrial radiation generates a quasi-stationary global climate state. However, natural causes such as volcanic eruptions or changes in the solar radiation as well as anthropogenic modifications of the atmospheric composition can perturb the global energy balance: the climate state gets out of balance. These external perturbations cause a net radiation flux change (in Wm^{-2}) which is defined as *radiative forcing*. (see review of Ponater et al., 2012)

Radiative forcing has been established as a good predictor of climate change. Several definitions of radiative forcing are available as shown in Fig.2.2. The so-called *stratosphere adjusted radiative forcing* is determined after the stratospheric temperature adapts to the external perturbation. This process is fast and happens within weeks to months. In contrast, the troposphere-surface system only adjusts over decades to millenia due to the slow response of the ocean. Hence, the stratospheric temperature change can be considered as part of the radiative forcing than as a response to the forcing. *Instantaneous radiative forcing* describes the resulting flux changes immediately after the perturbation is applied to the climate. Moreover, if the temperature in the troposphere and the stratosphere can adjust to the radiative perturbation but the surface temperature is held fixed, the flux change at TOA is defined as the *zero-surface-temperature-change radiative forcing*. Radiative forcings may be considered either at the tropopause or at the top of atmosphere (TOA). (Hansen et al., 1997; Stuber et al., 2001; Vial et al., 2013)

In this work the instantaneous radiative forcing at TOA is used as the most simple way to examine the reestablishment of the radiative equilibrium at TOA after applying an external perturbation.

To restore the radiative equilibrium at TOA, climate variables such as the surface temperature adapt and counteract the radiative forcing. A positive forcing (net downward flux change) implies a higher energy entry into the climate system inducing a warming. Following the Stefan-Boltzmann law the surface and atmospheric temperature rises until the outgoing longwave radiation balances the radiative forcing. Accordingly, a negative forcing produces a cooling. (Wallace and Hobbs, 2006; Zdunkowski et al., 2007)

The climate response can be described as a change in surface temperature ΔT_S^0 which, as a first approximation, varies linearly with the radiative forcing RF:

$$\Delta T_S^0 \approx \lambda_0 \cdot RF \tag{2.6}$$

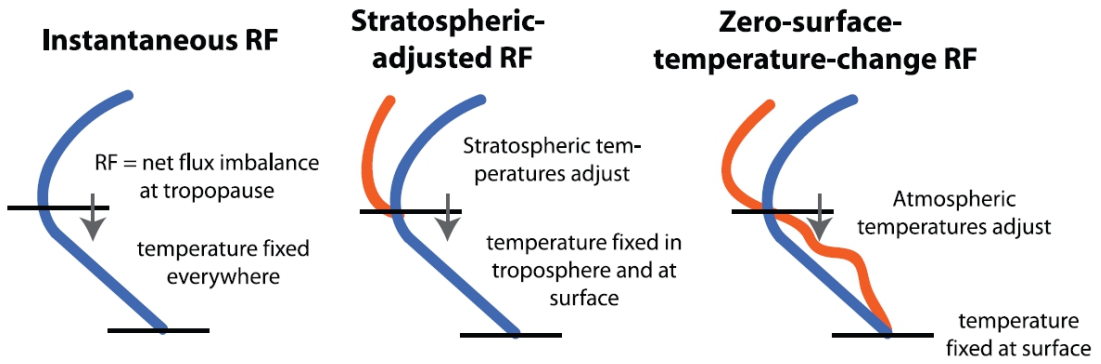

Figure 2.2: Schematic figure for the different definitions of radiative forcings. The lower line shows the surface, the upper line the tropopause. Blue lines represent the unperturbed and red lines the perturbed temperature profile. (IPCC, 2007)

The *climate sensitivity parameter* λ_0 thus describes the surface temperature change resulting from an applied radiative forcing (Ponater et al., 2012). If the climate sensitivity parameter is sufficiently independent from the applied perturbation and model, hence approximately constant, the radiative forcing would be a good indicator to forecast climate change, i.e. the change in the surface temperature ΔT_S. However, several studies have shown that the climate sensitivity parameter varies not only amongst models (Cess et al., 1990; Soden and Held, 2006), but also within in the same model, depending on the strength and the type of a given perturbation. The spatial structure of the perturbation in particular plays a major role (Berntsen et al., 2005; Stuber et al., 2005; Hansen et al., 1997).

2.3 Climate feedbacks

Surface temperature changes due to a radiative forcing also impacts other temperature dependent climate variables through physical or chemical processes. If those climate variables themselves are radiatively active, changes in their concentration and spatial structure influence in turn the Earth's radiation budget and thus produces an additional radiative flux change ΔR (see Fig. 2.3). This additional flux change adds on the original forcing to further changing the climate system and inducing further surface temperature change. Such climate variables are said to induce *feedbacks*. A feedback can either be positive which means that the radiative effect of the feedback amplifies the initial radiative perturbation or negative if the feedback dampens the radiative perturbation (Bony et al., 2006).

Considering the influence of the feedbacks, the total climate response ΔT_S can now be described as follows:

$$\Delta T_S \approx \lambda \cdot RF \tag{2.7}$$

where λ is the climate sensitivity parameter which considers the feedback processes as

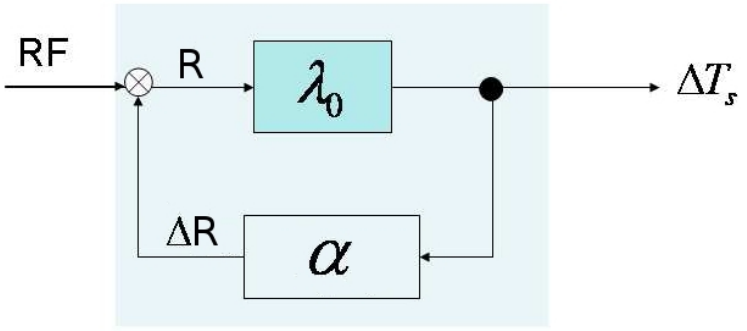

Figure 2.3: Schematic drawing of climate system with feedback loop. RF indicates the radiative forcing which induces a surface temperature change ΔT_S. Feedbacks α cause a net TOA flux change ΔR which forms together with the radiative forcing RF the total flux change R. λ_0 denotes the climate sensitivity parameter when no feedbacks are considered. (Dietmüller, 2011)

well.

To quantify feedback processes, the variable *feedback parameter* α is introduced. The feedback parameter describes the radiative effect of all feedbacks together and characterises the flux change due to a surface temperature increase. It is determined through the net TOA flux changes ΔR which is caused by the feedbacks:

$$\alpha = \frac{\Delta R}{\Delta T_S} \tag{2.8}$$

Under the assumption that all feedbacks are independent from each other, the feedback parameter can be written as the sum of the physical and chemical feedback parameters:

$$\alpha = \sum_i \alpha_i = \alpha_T + \alpha_q + \alpha_A + \alpha_C + \alpha_{O3} + \alpha_{CH4} + \alpha_{N2O} + \alpha_{CFC} \tag{2.9}$$

The physical feedback parameter are the temperature feedback α_T which describes the feedback due to the temperature response of the climate system, the water vapour feedback α_q, the surface albedo feedback α_A, and the cloud feedback α_C. The chemical feedbacks acts over radiatively active trace gases such as ozone (α_{O3}), methane (α_{CH4}), nitrous oxide (α_{N2O}), and chlorofluorocarbon (α_{CFC}). (Stuber, 2003; Schlesinger, 1988; Dietmüller, 2011)

This work will focus on physical feedbacks, namely temperature, water vapour, surface albedo and cloud feedback.

The temperature response of the climate can further be split up into the the so-called Planck feedback α_{pla}, the lapse rate feedback α_{lap}, and the stratospheric temperature feedback α_{str}: $\alpha_T = \alpha_{pla} + \alpha_{LR} + \alpha_{str}$.

The Planck feedback is the first order climate response to a radiative perturbation as it is described in Chap. 2.2. It dominates the temperature feedback. The Planck feedback

describes the homogeneous change of the temperature throughout the troposphere. The troposphere is assumed to be perfectly mixed. Hence, an increase in surface temperature is passed to all layers of the troposphere through convection. According to the Stephan-Boltzmann law, the homogeneous increase of the tropospheric temperature rises the emitted longwave radiation of the troposphere to space. Thus, the Planck feedback counteracts the initial perturbation. It is the strongest negative feedback (Soden and Held, 2006).

The lapse rate feedback specifies the radiation effect of the change of the tropospheric lapse rate due to a perturbation. If the lapse rate decreases in response to a warmer climate, the temperature in the upper troposphere increases more than in the lower troposphere. Thus the stronger temperature increase in upper troposphere leads to an enhanced longwave radiation emission to space which cools the atmosphere. The lapse rate feedback is then negative. In contrast, an increase of the lapse rate in a warmer climate causes less longwave emission to space. More energy is trapped in the atmosphere resulting in an enhanced greenhouse effect which warms the atmosphere. The lapse rate feedback is therefore positive. (Colman, 2002)

The radiative effects resulting from temperature changes which occur above the tropopause are summarized in the stratospheric temperature feedback. The stratospheric temperature change can be regarded separately because it is decoupled from the tropospheric convection and mixing. If the stratospheric temperature adjustment is included in the radiative forcing calculations, the stratospheric temperature feedback would be counted as part of the radiative forcing. The stratosphere adjusted radiative forcing contains already the temperature change which takes place in the stratosphere. This work only examines the instantaneous radiative forcing and feedbacks. To include all components of the temperature response, the stratospheric temperature change is considered in the stratospheric temperature feedback.

Increased atmospheric temperature as a result of an external radiative forcing leads to an increase of the water vapour uptake in the atmosphere. This relation is explained by the Clausius-Clapeyron equation, which describes the saturation water vapour pressure as nearly exponential with temperature. Theory of a well mixed troposphere suggests, and experience with climate models confirms, that the relative humidity within the troposphere stays almost constant if tropospheric temperature is changed. In addition, water vapour is a strong greenhouse gas, absorbing predominantly in the longwave region. Consequently, higher water vapour concentrations in the atmosphere increase the absorption of longwave radiation inducing a further warming of the climate. Hence, the water vapour feedback is positive. It is by far the strongest feedback acting in the atmosphere. For example, in the case of a doubling of atmospheric carbon dioxide concentration, the water vapour feedback alone increases the global temperature response by a factor of two. (Wallace and Hobbs, 2006; Bony et al., 2006)

Snow and ice reflect incident solar radiation. Through global warming, the surface area covered with snow and ice decreases, so less solar radiation is reflected back to space. The ground absorbs more radiation causing the surface temperature to rise. Thus, the surface albedo feedback is positive because the initial warming is enforced. Sea ice changes account for 55% of the surface albedo feedback whereas snow changes contribute

45%. (Bony et al., 2006; Colman, 2002)

Clouds participate in the shortwave and longwave radiation transfer: they reflect shortwave and trap longwave radiation. Cloud optical properties, cloud amount and vertical distribution of clouds determine these two competing radiative effects and thus define the net radiative influence of clouds acting on the climate system. To understand the cloud feedback, it is necessary to understand how climate change will affect these properties of different cloud types. For example, thin cirrus clouds warm the Earth's system as they transmit nearly all solar radiation, but absorb strongly the terrestrial radiation, strengthening Earth's greenhouse effect. In contrast, subtropical stratocumulus decks cool the Earth as their cooling effect due to the reflection of solar radiation back to space overweighs their contribution to Earth's greenhouse effect. For anvil clouds in the tropical deep convective regime, shortwave and longwave contribution almost compensate each other. (Wallace and Hobbs, 2006; Bony et al., 2006)

The water vapour and lapse rate feedback are often considered together (Colman, 2003; Held and Soden, 2000). Both feedbacks are known to be anticorrelated: if the water vapour feedback is strongly positive, the lapse rate feedback is also strongly negative, although the magnitude of the lapse rate feedback remains smaller than the magnitude of the water vapour feedback. Thus the combined water vapour and lapse rate feedback is positive. A possible explanation for the anticorrelation could be that both feedback mechanism are associated with the same process: the deep convection in the tropical troposphere. Global warming enhances the tropical deep convection which transports more heat to the upper troposphere. On the one hand, this reduces the lapse rate, leading to a stronger negative lapse rate feedback. On the other hand, the water vapour concentration in the upper troposphere increases which strengthens the positive water vapour feedback. This anticorrelation seems to affect the intermodel spread of the combined water vapour and lapse rate feedback which is reduced by a factor of two compared to the intermodel spread of the separately considered feedbacks (Bony et al., 2006).

3 Feedback analysis method and model description

3.1 "Partial Radiative Perturbation"-Method

To determine the feedback parameters for the individual feedbacks, the "Partial Radiative Perturbation"-method (PRP-method) is used. This method was first introduced by Wetherald and Manabe (1988).

Feedbacks counteract an external forcing by changing the flux at top of atmosphere (TOA) to restore radiative equilibrium. For a sufficiently small perturbation, it is assumed that the feedbacks are independent and can be considered separately. Combining Eq. 2.8 and 2.9, the feedback parameter for one particular feedback process x is obtained as follows:

$$\alpha_x = \frac{\Delta R_x}{\Delta T_S} \tag{3.1}$$

with ΔR_x being the TOA radiative flux change due to this particular feedback.

To retrieve the net TOA flux changes ΔR_x due to a specific feedback, for example water vapour feedback, two offline radiative transfer calculations need to be performed. First, variables such as water vapour q, cloud parameters C, surface albedo A, and temperature profil T are taken from the control simulation and the net TOA flux $R(q_{ref}, C_{ref}, A_{ref}, T_{ref})$ is obtained. For the second calculation, all variables stay unchanged, except for one variable, here water vapour, is substituted by the water vapour q from the (perturbed) climate change simulation. Then, again, the net TOA flux is determined $R(q_{per}, C_{ref}, A_{ref}, T_{ref})$. To obtain the net flux change due to the water vapour feedback, the results of both radiative transfer calculations are subtracted:

$$\Delta R_q = R(q_{per}, C_{ref}, A_{ref}, T_{ref}) - R(q_{ref}, C_{ref}, A_{ref}, T_{ref}) \tag{3.2}$$

According to Eq. 3.1, the feedback parameter can be now calculated. The annual mean flux changes ΔR_q are divided by the annual mean temperature changes ΔT_S and then averaged over several simulation years to consider the interannual variability of the flux and surface temperature change. Using this method, one variable after the other is substituted to determine the corresponding feedback parameters.

Aires and Rossow (2003) pointed out that the assumptions of linearity and separability might cause problems. As the initial perturbation is only applied to one variable at a time, possible interactions with other variables are neglected. A further problem is that the radiative perturbation resulting from a parameter change (e.g., from a changed water vapour distribution) may depend on the climate state to which it is applied.

Thus, Colman and McAvaney (1997) suggested to compute the PRP-method twice to reduce the decorrelations and the dependences between the feedback processes. First, a variable from the climate change simulation is substituted into the reference climate. According to Eq. 3.2, the flux change of, for example, the water vapour feedback is calculated as $\Delta R_q^{FW} = R(q_{per}, C_{ref}, A_{ref}, T_{ref}) - R(q_{ref}, C_{ref}, A_{ref}, T_{ref})$. Within this thesis, this way of calculating ΔR_q^{FW} will be called the forward PRP calculation. Second, a climate variable from the reference climate is substituted into the perturbed climate which is called the backward PRP calculation. The flux change of the water vapour feedback is determined as $R(q_{ref}, C_{per}, A_{per}, T_{per}) - R(q_{per}, C_{per}, A_{per}, T_{per})$. Note that if a feedback process leads to a positive flux change at TOA for the FW PRP calculation, it will cause a negative flux change for the BW PRP calculation. To be able to compare both PRP calculations, the flux changes of the BW PRP calculation are multiplied by -1: $\Delta R_q^{BW} = -(R(q_{ref}, C_{per}, A_{per}, T_{per}) - R(q_{per}, C_{per}, A_{per}, T_{per}))$. Then the average of the flux changes obtained from the forward (FW) and the backward (BW) PRP calculations is formed: $\frac{1}{2}(\Delta R_q^{FW} + \Delta R_q^{BW})$. In this work, the combination of FW and BW PRP calculations will be denoted as (FW+BW) PRP calculation.

However, this method is computationally very expensive because offline calculations have to be performed for each feedback. Nevertheless, the PRP-method is used in this work since this method provides the possibility of a full feedback analysis. In particular, the cloud feedback alone can be considered here whereas other feedback analysis methods do not support this: The cloud feedback either cannot be determined at all (Stuber-method) or can only be calculated as a residuum of all other feedbacks (e.g. radiative kernels, Soden and Held (2006)). Due to the separation approach we are able to investigate all feedbacks individually.

It should be noted that the individual feedback parameters cannot be compared against observation. Hence, a validation of the feedback parameters calculated by the PRP-method is not possible.

3.2 Model and simulation set-up

Carbon dioxide driven simulations with the interactively coupled climate chemistry model EMAC/MLO were performed by Dietmüller (2011). EMAC (**E**CHAM5/**M**ESSy **A**tmospheric **C**hemistry) describes the processes in the troposphere and middle atmosphere. The core atmospheric model of EMAC contains the general circulation model ECHAM5 and, in particular, uses its radiation parameterisation scheme. A mixed layer ocean (MLO) with a depth of 50 m was coupled to EMAC. (Dietmüller, 2011, and references therein)

Several simulations forced by increased atmospheric CO_2 concentrations with interactively coupled atmospheric chemistry (*chem*) and without interactively coupled chemistry (*nochem*) were conducted and are available for evaluation in this thesis. The initial CO_2 concentration of 367 ppmv was (a) increased by 75 ppmv to a value of 442 ppmv, (b) doubled to a value of 734 ppmv, and (c) quadrupled to 1468 ppmv. The reference simulation specify the mean climate state of the year 2000. After the CO_2 increase was applied

abruptly to the reference climate state, the simulations were run for 40 model years until a new equilibrium state is reached. Only those model years which achieved the new equilibrium state can be used for a feedback analysis. Since for a small perturbation, the equilibrium state is reached earlier (as can be seen in Fig. 8.2 Dietmüller (2011)), more model years are available for a feedback analysis than for a large perturbation. The corresponding stratosphere adjusted radiative forcings, the temperature increases and the climate sensitivity parameters for the three types of CO_2 driven simulations reported by Dietmüller (2011) are listed in the Tab. 3.1.

Experiment	CO_2 [ppmv]	RF_{adj} [Wm^{-2}]	ΔT_S [K]	λ_{adj} [K/Wm^{-2}]
(a) 442CO2	442	1.06	0.78	0.73 ± 0.06
(b) 2xCO2	734	4.13	2.91	0.70 ± 0.02
(c) 4xCO2	1468	8.93	8.13	0.91 ± 0.01

Table 3.1: CO_2 concentration, stratosphere adjusted radiative forcing RF_{adj}, surface temperature increase ΔT_S and climate sensitivity parameter λ_{adj} (with corresponding 95% confidence intervals) for the simulations (a) 442CO2 (corresponds to an increase of the CO_2 by 75 ppmv to a value of 442 ppmv), (b) 2xCO2 (corresponds to a doubling of CO_2), and (c) 4xCO2 (corresponds to a quadrupling of the CO_2). The variables are given for the simulation without interactively coupled atmospheric chemistry *nochem.* (Dietmüller, 2011)

Further description of the model and the simulation results can be found in Dietmüller (2011).

To perform the offline radiative transfer calculations for the feedback analysis (see Chap. 3.1), the single column radiation code was isolated from the model ECHAM5 (or EMAC, see above) by Klocke (2011). Technically, the code version used here is called ECHAM5.4. It contains 16 longwave and 6 shortwave bands and thus, for practical purposes, it can be assumed that the radiation code is almost identical with the radiation code used by Dietmüller (2011). This is important to maintain consistency with the simulation Dietmüller (2011) performed.

Instantaneous output variables such as temperature profile, specific and relative humidity, albedo, cloud properties, tropopause level and trace gas concentrations (ozone, methane, nitrous oxide) of the CO_2 driven simulations performed by Dietmüller (2011) are taken as input variables for the separated radiation transfer model. The calculations are executed twice per day: at 00:00 and 12:00 UTC. The radiative transfer models determined the fluxes for "all sky" (including clouds) and "clear sky" (excluding clouds) at each of the 41 atmospheric layers as well as at the tropopause and the surface.

3.3 Separation of feedback processes

According to Eq. 3.2, to determine the cloud feedback, cloud variables such as cloud cover, cloud droplet number concentration, liquid and ice water content are substituted. These variables are used to calculate the cloud optical properties such as optical thickness and emissivity. The temperature is not only essential for the longwave radiative transfer but also influence the calculation of the cloud optical properties such as the optical thickness. A change in the temperature profile would as well change the optical properties of the clouds and thus the latter would be misleadingly accounted to the temperature response. Therefore, for this thesis, the temperature induced change of cloud optical properties has been split up from the temperature feedback and added to the cloud feedback.

Equivalently, modifications have been made concerning the clear-sky optical thickness. The clear-sky optical thickness is calculated as a sum of absorption coefficients of various greenhouse gases as well as the absorption effect of the water vapour self-continuum. In addition, it also depends on the temperature. Thus a change of the temperature, due to a radiative forcing, modifies the water vapour self-continuum and thereby the clear-sky optical thickness. Hence, a change in the clear-sky optical thickness caused by a change in the water vapour self-continuum would be accounted to the temperature feedback. To avoid this, this effect is split up from the rest of the calculation of the clear-sky optical thickness and added to the water vapour feedback. Thus the water vapour feedback does not only consist of the change in water vapour mixing ratio but also of the change in the emissivity.

This modification of the original program code has been motivated by the consideration that shortwave contributions to the feedbacks controlled by temperature ($\alpha_{pla}, \alpha_{LR}, \alpha_{str}$, see above) seem physically unreasonable, if they are caused by numerically artificial changes in shortwave cloud optical parameters. These ought to be included in the cloud feedback rather than in Planck or lapse rate feedback. However, for the quantitative results of the calculated feedbacks, these changes are not of substantial relevance.

4 Results

4.1 Climate feedbacks of CO_2 doubling simulation

This section describes the feedbacks for the case of a doubled atmospheric CO_2 simulation. Several studies have already investigated feedbacks in CO_2 doubling simulations using the PRP-method (Soden and Held, 2006; Colman, 2003; Klocke et al., 2013). This gives a good opportunity to compare the results obtained here from the model EMAC with other studies.

Fig. 4.1 shows the global distributions of the feedback parameter of the various feedbacks. Results are presented as the average of the calculations yielded by the FW and BW PRP calculation (Chap. 3.1). Positive values indicate an increased downward radiation at TOA inducing an energy gain for the climate system and thus a warming. To determine the mean feedback parameters and their statistical uncertainty as precisely as possible, they are averaged over 24 years and their corresponding interannual standard deviation is calculated. According to *Student's t-test* (e.g. Kreyszig (1979)), a 95% confidence interval for the feedback parameters is determined. The globally averaged shortwave and longwave components of the feedback parameters and their standard deviations are listed in Tab. 4.1 for the FW, BW and the combined (FW+BW) PRP calculations. Furthermore, the net feedback parameters are given being the sum of the shortwave and longwave component.

The Planck feedback with a 95% confidence interval (calculated by means on the interannual standard deviation) of (-3.10 $\pm$ 0.01) $Wm^{-2}K^{-1}$ is strongly negative and dominates the climate response to an external forcing. It acts only in the longwave spectral region. The global distribution of the TOA flux changes (Fig. 4.1) closely relates to the pattern of the surface temperature change due to a doubling of CO_2 (shown in Fig. A.1). Large surface warming occurs in the high latitudes, especially over land and sea ice regions. The Planck feedback shows maximum negative values in the same areas. Slight flux changes are generally found in the tropics and over the oceans where also small increase in the surface temperature occurs. Soden and Held (2006) report a multimodel mean and intermodel standard deviation for the Planck feedback of (-3.21 $\pm$ 0.04) $Wm^{-2}K^{-1}$ which is slightly higher than the value found here.

The contribution to the global lapse rate feedback has a very distinct pattern: at high latitudes, the lapse rate feedback is positive while at low latitudes it is negative. This structure can also be explained by the the structure of the temperature change (Fig. A.2). At low latitudes, the temperature in higher altitudes increases stronger than in lower altitudes, creating a decrease of the lapse rate and thus leading to a negative feedback. Whereas at high latitudes, the temperature increase is stronger near the surface, consequently inducing an increase of the lapse rate and producing a positive feedback. Overall,

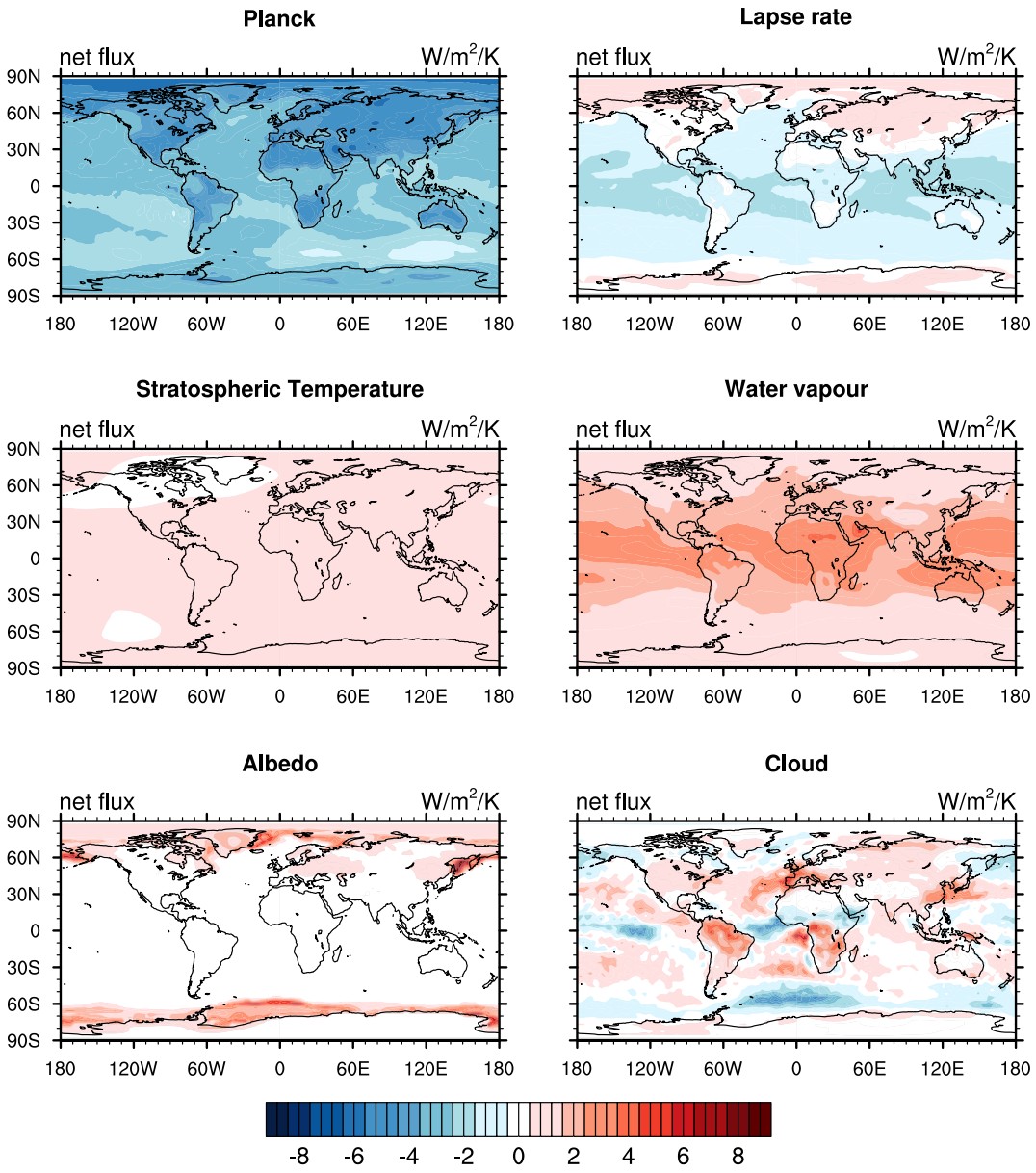

Figure 4.1: Global distribution of net Planck, lapse rate, stratospheric temperature, water vapour, albedo, and cloud feedback parameters for CO_2 doubling at TOA for the combined (FW+BW) PRP calculation. Positive values denote an increased downward radiation. The simulation *nochem* is displayed.

α_x	PRP calculation	SW	SW std	LW	LW std	net	net std
α_{pla}	FW PRP	0	0	-3.21	0.02	-3.21	0.02
	BW PRP	0	0	-2.99	0.02	-2.99	0.02
	(FW+BW) PRP	0	0	-3.10	0.02	-3.10	0.02
α_{LR}	FW PRP	0	0	-1.35	0.09	-1.35	0.09
	BW PRP	0	0	-0.37	0.09	-0.37	0.09
	(FW+BW) PRP	0	0	-0.86	0.09	-0.86	0.09
α_{str}	FW PRP	0	0	0.50	0.02	0.50	0.02
	BW PRP	0	0	0.62	0.03	0.62	0.03
	(FW+BW) PRP	0	0	0.56	0.02	0.56	0.02
α_A	FW PRP	0.26	0.02	0	0	0.26	0.02
	BW PRP	0.21	0.02	0	0	0.21	0.02
	(FW+BW) PRP	0.23	0.02	0	0	0.23	0.02
α_q	FW PRP	0.37	0.01	2.14	0.07	2.51	0.08
	BW PRP	0.34	0.01	1.18	0.07	1.52	0.08
	(FW+BW) PRP	0.36	0.01	1.66	0.07	2.01	0.08
α_C	FW PRP	-0.10	0.15	0.68	0.05	0.57	0.13
	BW PRP	-0.16	0.15	0.16	0.05	0.00	0.14
	(FW+BW) PRP	-0.13	0.15	0.42	0.05	0.29	0.13

Table 4.1: Shortwave (SW), longwave (LW), and net (sum of SW and LW) feedback parameters and corresponding standard deviation (std) for CO_2 doubling at TOA (*nochem* simulation). Values are given for the FW, BW and the combined (FW+BW) PRP calculations. Unit: $Wm^{-2}K^{-1}$

the global average is negative and has a value of (-0.86 ± 0.04) $Wm^{-2}K^{-1}$ which is in very good agreement with the intermodel mean of (-0.84 ± 0.26) $Wm^{-2}K^{-1}$ reported by Bony et al. (2006)[1] .

A very homogeneous global distribution is shown by the stratospheric temperature feedback. Mainly due to a CO_2 doubling, the stratosphere cools (see Fig. A.2) and produces a positive flux change at TOA. The feedback parameter has a value with corresponding 95% confidence interval of (0.56 ± 0.01) $Wm^{-2}K^{-1}$.

The increase of water vapour all over the atmosphere for a doubling of CO_2 causes a positive feedback. With (2.01 ± 0.03) $Wm^{-2}K^{-1}$, it is the strongest positive feedback and slightly higher than the multi-model mean of (1.80 ± 0.18) $Wm^{-2}K^{-1}$ (Bony et al., 2006). Maximum values are found in the tropics where the specific humidity has its largest increase due to global warming (Fig. A.3). Moreover, the longwave contribution dominates the feedback with 82%, whereas the shortwave radiation only contributes 18% to the global feedback parameter.

The water vapour feedback can be further split up in the feedback due to tropospheric and stratospheric water vapour changes since they are controlled by different physical mechanisms. The tropospheric water vapour feedback dominates over the stratospheric water vapour feedback by 85%. Fig. A.3 shows that the highest increase of water vapour happens in the troposphere.

Radiative perturbations due to surface albedo are only found at high latitudes where the albedo changes in a warmer climate due to melting of ice and snow. In the Southern Hemisphere, radiative perturbations are limited only to Antarctic sea ice. Although, the albedo feedback can locally reach values up to 9 $Wm^{-2}K^{-1}$, its global average is small with (0.23 ± 0.01) $Wm^{-2}K^{-1}$. This is in good agreement with the multi-model mean of (0.26 ± 0.08) $Wm^{-2}K^{-1}$ (Bony et al., 2006).

Finally, the cloud feedback is shown in Fig. 4.1. Locally high positive and negative flux changes up to 8 $Wm^{-2}K^{-1}$ appear. Especially the strong negative TOA flux change over the South Atlantic Ocean is remarkable. Large positive flux changes occur over Europe, South Africa and South America. But the global average takes a comparatively small value of (0.29 ± 0.06) $Wm^{-2}K^{-1}$ which just remains within the relatively broad range of the multi-model mean (0.69 ± 0.38) $Wm^{-2}K^{-1}$ (Bony et al., 2006).

The shortwave and longwave component of the cloud feedback have opposite signs. Through a doubling of CO_2 concentration, the clouds reflect more solar radiation back to space. The shortwave component of the cloud feedback is negative and has a value with corresponding 95% confidence interval of (-0.13 ± 0.06) $Wm^{-2}K^{-1}$ (see Tab. 4.1). In contrast, a doubling of the CO_2 concentrations seems to enhance the cloud's greenhouse effect by trapping more longwave radiation. A possible reason could be an increase in the cover of high clouds. Thus the longwave component of the cloud feedback warms the climate with (0.42 ± 0.02) $Wm^{-2}K^{-1}$. Overall, the longwave cloud feedback is three

[1]The feedback parameters determined in this work are always denoted with the 95% confidence interval which is calculated by means of the interannual standard deviation. Thus, the range of the feedback parameters indicates the interannual variability. The feedback parameters are compared with intermodel means reported by Soden and Held (2006) and Bony et al. (2006). Their standard deviations describe the intermodel spread of the feedback parameters.

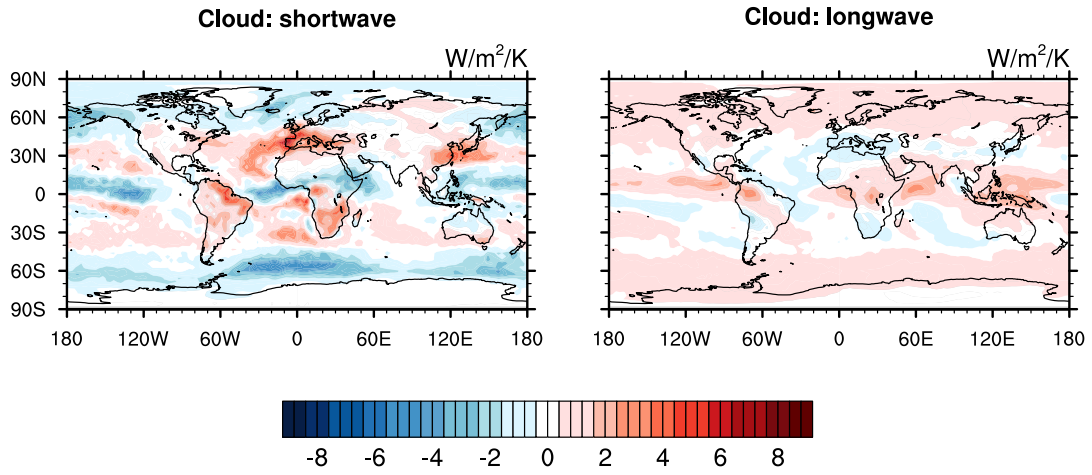

Figure 4.2: Global distribution of shortwave and longwave feedback parameter of the cloud feedback for a doubling of CO_2 at TOA (*nochem* simulation). Unit: $Wm^{-2}K^{-1}$

times larger than the shortwave component and dominates the global mean value. The net cloud feedback is positive and therefore enhance the global warming. Fig. 4.2 shows the spatial distribution of the shortwave and longwave cloud feedback. Although the sign of the global mean value is determined by the longwave component, the spatial structure of the cloud feedback is dominated by the shortwave part. The structure of the longwave cloud feedback is rather homogeneous whereas the shortwave component presents a significant pattern with strong maxima and minima which moulds the spatial structure of the net cloud feedback.

4.2 Temporal variability of climate feedbacks

As the climate state varies strongly from year to year, it is challenging to extract the small effect of a radiative perturbation due to a feedback process from the high interannual variability. Consequently, the feedbacks also show a high year-to-year variability. Fig. 4.3 presents the temporal variability of the global averaged feedback parameters for 24 years. The grey shaded area indicates one standard deviation (reported in Tab. 4.1). For the Planck, the stratospheric temperature, and the albedo feedback, the year-to-year variability is very small in absolute as well as in relative terms. However, for all other feedbacks, the feedback parameters deviate considerably from year to year. Their standard deviation is about five times higher than of, e.g. the Planck feedback and has a value of approximately 0.1 $Wm^{-2}K^{-1}$. The cloud feedback in particular shows a high standard deviation which is about 50% of the feedback parameter itself. The high standard deviation mainly originates from the shortwave component. This is in agreement with results by Klocke et al. (2013).

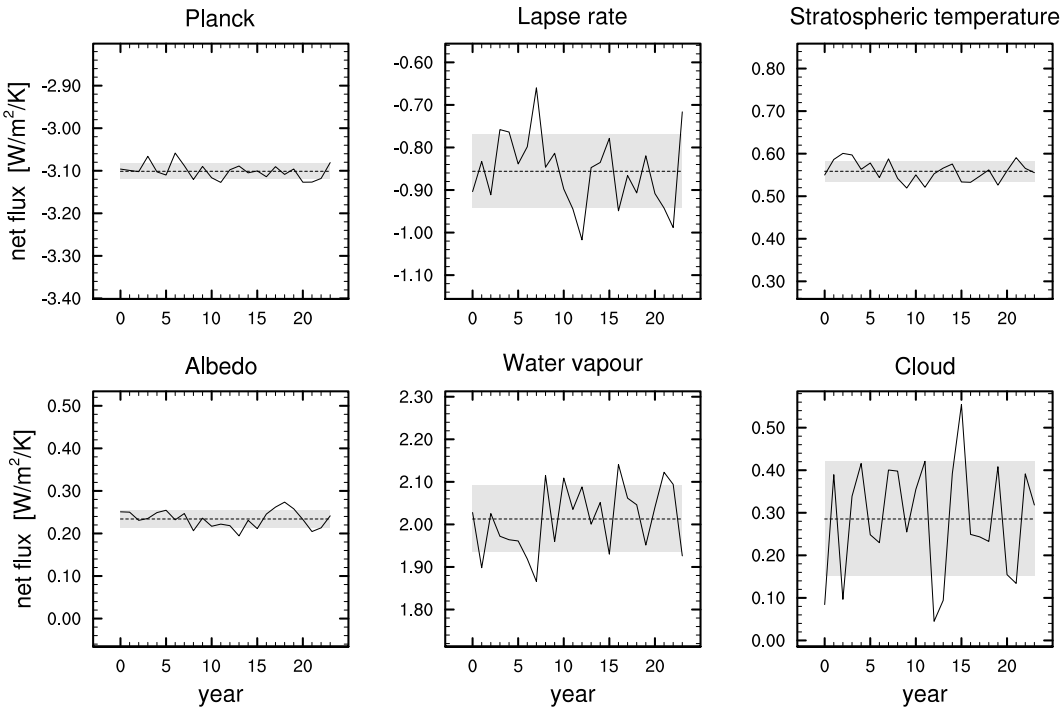

Figure 4.3: Temporal variability of global averaged climate feedback parameters over 24 years for a CO_2 doubling (*nochem* simulation). Values are given for the (FW+BW) PRP calculation. The grey shaded area indicates one standard deviation. Unit: $Wm^{-2}K^{-1}$

The FW and BW PRP calculations show the same standard deviations for a particular feedback parameter (Tab. 4.1). Further, the combination of both PRP calculations has no significant effect on the standard deviation.

The mean values of the feedback parameters strongly depend on the considered ensemble of simulation years. For example, the mean value of the water vapour feedback parameter differs considerably if either the first five or the last five years are considered.

Whenever feedback parameters are used to compare or explain phenomena, one has to keep in mind that the feedback parameter consists of an ensemble of strongly varying values and that the mean values may depend on the considered simulation years. Hence, it is important to have an ensemble of evaluated years which is large enough to reliably determine feedback parameters as to keep their statistical uncertainty as low as possible.

4.3 Comparison of feedbacks between simulations with and without interactively coupled atmospheric chemistry

The feedbacks considered in the previous sections describe the simulations without interactively coupled atmospheric chemistry (*nochem*). Now, they will be compared to feedbacks corresponding to the simulations with interactively coupled chemistry (*chem*) which were also performed by Dietmüller (2011). In these simulations the atmospheric chemistry could adjust to the applied perturbation. Trace gases such as ozone, methane and nitrous oxide could change their concentrations and hence influence the radiation transfer in the atmosphere. Following Dietmüller (2011, Tab. 8.1), the climate sensitivity parameter may vary significantly between the simulation *nochem* and *chem* for the same strength of CO_2 forcing. Hence, feedback analyses could be expected to be helpful for interpreting these differences, too.

Tab. 4.2 compares the 95% confidence intervals of the feedback parameters for the 2xCO2 simulations with and without interactively coupled chemistry. The values of the *nochem* case are taken from Tab. 4.1 and presented again here to be able to compare better between the two simulation types. According to Dietmüller et al. (2014), the climate sensitivity parameters of these simulations are just marginally different on a 95% significance basis. For a doubling of CO_2, the stratosphere adjusted climate sensitivity parameter for the *nochem* simulation is found in the range [0.69; 0.72] K/Wm^{-2} whereas for the *chem* simulation, it has a range of [0.66; 0.69] K/Wm^{-2}.

α_x	*nochem* simulation	*chem* simulation
α_{pla}	-3.10 ± 0.01	-3.10 ± 0.01
α_{LR}	-0.86 ± 0.04	-0.88 ± 0.04
α_{str}	0.56 ± 0.01	0.43 ± 0.01
α_q	2.01 ± 0.03	2.01 ± 0.04
α_A	0.23 ± 0.01	0.23 ± 0.01
α_C	0.29 ± 0.06	0.35 ± 0.05

Table 4.2: Feedback parameters for doubling CO_2 simulations without interactively coupled (*nochem*) and with interactively coupled (*chem*) chemistry for the (FW+BW) PRP calculation. Given are the 95% confidence intervals. The values for the simulations without interactively chemistry are taken from Tab. 4.1. Unit: Wm^{-2}K^{-1}

For most feedbacks, no significant changes are found. The Planck, lapse rate, water vapour, surface albedo and cloud feedback agree within their 95% confidence intervals. The simulation runs *nochem* and *chem* cannot be distinguished significantly for these feedbacks. Only the stratospheric temperature feedback differs when the interaction with the atmospheric chemistry is taken into account. The feedback parameter of the

simulation *chem* disagree by about 23% from the value of the simulation *nochem*. The stratospheric temperature feedback thus depends strongly on the presence of interactive atmospheric chemistry.

A possible explanation for this behaviour is the change in stratospheric ozone due to a CO_2 radiative forcing which dominates the stratospheric temperature modification. The effect of other trace gases such as methane and nitrous oxide can be neglected (Dietmüller, 2011). When ozone is able to adjust to the radiative perturbation, it will decrease in the tropical lower stratosphere and increase in the rest of the stratosphere (see Fig. A.4, Dietmüller et al. (2014)). An ozone increase leads to more absorption of shortwave radiation, heating the air temperature and hence, increasing the longwave emission. In contrast, less shortwave radiation can be absorbed when ozone is decreased, thus cooling the air and reducing the longwave emission. This leads to a similar pattern for the stratospheric temperature change due to ozone changes: in the tropical lower stratosphere the stratospheric temperature decrease over 1 K, whereas in the upper stratosphere it increases by over 2 K (see Fig. A.5). This temperature increase in the upper stratosphere due to ozone changes leads to an increase of longwave emission. Thus the ozone change due to a doubling of CO_2 acts like a negative feedback (Dietmüller et al., 2014) which reduces the positive stratospheric temperature feedback when the interaction of atmospheric chemistry is considered and trace gases could adjust to the radiative perturbation.

4.4 Additivity of climate feedbacks

Radiative feedbacks develop as a consequence of parameter changes induced by a radiative forcing in order to restore the radiative balance at TOA. Consequently, the sum of all feedback parameters should exactly balance the radiative forcing: $\sum_x \alpha_x = -\frac{RF}{\Delta T_S}$. In Fig. 4.4, the absolute values of the feedbacks' sum and the radiative forcing are displayed for the FW, the BW and the combined (FW+BW) PRP calculations when the atmospheric CO_2 is doubled. Furthermore, the *total feedback* is plotted in Fig. 4.4. To calculate the total feedback for the FW PRP calculation, all feedback relevant variables of the reference simulation are substituted at once by the variables of the climate change simulation and not one by one as it is done to determine one individual feedback; vice versa for the BW PRP calculation (see Chap. 3.1). In case of perfect independence of the individual feedbacks, as assumed by the feedback theory, the total feedback α and the sum of feedbacks should agree (Eq. 2.9).

For the FW PRP calculation, neither the sum of the feedbacks nor the total feedbacks agree very well with the radiative feedback. Further, the total feedback does not correspond to the sum of feedbacks. Considering the BW PRP calculation, the mean value of the feedbacks' sum equals the radiative forcing nicely, but the total feedback does not agree with either. Only the combined (FW+BW) PRP calculation shows an almost perfect agreement of the radiative forcing, the sum of the feedbacks, and the total forcing and hence, meets the theoretical expectations. The difference between the total feedback and the sum of the feedbacks is with 0.01 $\mathrm{Wm^{-2}K^{-1}}$ negligibly small.

The climate response to a radiative perturbation is best described by the (FW+BW)

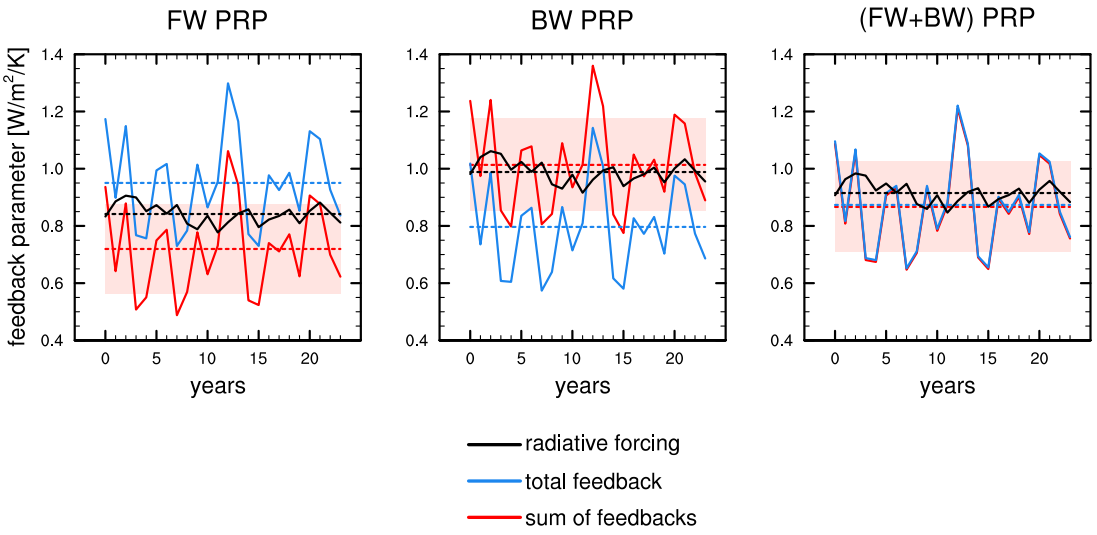

Figure 4.4: Sum of the individual feedbacks, total feedback, and the radiative forcing in $Wm^{-2}K^{-1}$ are shown for a doubling of the atmospheric CO_2. The FW, BW, and (FW+BW) PRP calculations for the *nochem* simulation are presented for 24 years. Only absolute values are plotted to compare the magnitudes of the sum and the total feedback with the radiative forcing. The dashed lines indicate the ensemble mean values. The red shaded area represents the standard deviation of the sum of the feedbacks.

PRP calculation. The disagreement between the climate feedbacks and the radiative forcing is only 0.05 $Wm^{-2}K^{-1}$. This accounts for 5% of the forcing. The existence of a residual term was already pointed out by Shell et al. (2008) who claim that it would be small with about 10%. Further, Klocke et al. (2013) report a residual term for the PRP-method which has a magnitude of 9%. Compared to these values, the residual term in this work is small. After the climate was perturbed, the radiative equilibrium is fully restored. The climate response can be completely described by the sum of the individual feedbacks because all existing feedbacks of the *nochem* simulations are covered in the sum of the physical feedbacks.

Moreover, the additivity of feedbacks which is the basic assumption of the PRP-method (Eq. 2.9), is only valid for the (FW+BW) PRP calculation. Here, the sum of the feedbacks perfectly equals the total feedback. When simply the FW or BW PRP calculation is considered, the sum differs from the total feedback by about 0.25 $Wm^{-2}K^{-1}$. In these cases, the sum of the feedbacks may not include all components of the climate response. Possible missing parts could be interaction between feedbacks which are neglected when feedbacks are considered individually.

To further investigate the possibility of feedback interactions, selected combinations of feedbacks are analysed. For this purpose, the sum of the selected individual feed-

backs is compared with the feedback obtained when all relevant climate variables of the reference simulation are substituted at once by the variables of the climate change simulation and vice versa. For example, the net flux change for the combined water vapour and cloud feedback would be calculated as $\Delta R_q = R(q_{per}, C_{per}, A_{ref}, T_{ref}) - R(q_{ref}, C_{ref}, A_{ref}, T_{ref})$ for the FW PRP calculation (see Chap. 3.1). The results for the combined temperature components, the combined water vapour and lapse rate, the combined albedo and cloud, the combined water vapour and cloud and finally the combined Planck and water vapour feedbacks are listed in Table 4.3.

Combinations of feedbacks		FW PRP	Diff	BW PRP	Diff	(FW+BW) PRP	Diff
Temperature	$\alpha_{pla}+\alpha_{LR}+\alpha_{str}$	-4.06		-2.74		-3.40	
	$\alpha_{(pla+LR+str)}$	-4.03	-0.03	-2.80	0.06	-3.42	0.02
Water vapour +	$\alpha_q+\alpha_{LR}$	1.16		1.15		1.16	
Lapse rate	$\alpha_{(q+LR)}$	1.38	-0.22	0.94	0.22	1.16	0.00
Albedo +	$\alpha_A+\alpha_C$	0.83		0.21		0.52	
Cloud	$\alpha_{(A+C)}$	0.78	0.05	0.25	-0.05	0.52	0.00
Water vapour +	$\alpha_q+\alpha_C$	3.08		1.52		2.30	
Cloud	$\alpha_{(q+C)}$	1.82	1.26	2.77	-1.25	2.30	0.00
Planck +	$\alpha_{pla}+\alpha_q$	-0.71		-1.47		-1.09	
Water vapour	$\alpha_{(pla+q)}$	-0.61	-0.10	-1.53	0.06	-1.07	-0.02

Table 4.3: Overlapping effects of FW, BW, and combined (FW+BW) PRP calculations are shown for selected combinations of feedbacks of the *nochem* 2xCO2 simulation. The sum of the individual feedback is compared to the combination of the particular feedbacks. The difference of the sum and combined feedback is presented in the column "Diff". Unit: $Wm^{-2}K^{-1}$

To calculate the complete temperature feedback, Planck, lapse rate, and stratospheric temperature feedbacks are added obtaining a value of -4.06 $Wm^{-2}K^{-1}$ for the FW PRP calculation. The combination of all three feedbacks together results in a feedback parameter of -4.03 $Wm^{-2}K^{-1}$. The difference between these two methods is with -0.03 $Wm^{-2}K^{-1}$ very small. Also, the BW PRP calculation yields a small difference of 0.06 $Wm^{-2}K^{-1}$. The last column in Tab. 4.3 denotes the difference between the sum of the individual feedbacks and the combinations of the feedbacks for the (FW+BW) PRP calculation. Here, the difference for the (FW+BW) PRP calculation is 0.02 $Wm^{-2}K^{-1}$. For the case of the temperature feedback the deviation of the sum and the combination of the feedbacks is negligible small. Consequently, the temperature related feedback parameters

are additive and no error is made through their separation.

The sum of the water vapour and lapse rate feedback $\alpha_q + \alpha_{LR}$ provides an almost identical value of 1.16 $\mathrm{Wm^{-2}K^{-1}}$ for the FW and BW PRP calculations, whereas the combined water vapour and lapse rate feedback $\alpha_{(q+LR)}$ deviates by almost 20% from the sum $\alpha_q + \alpha_{LR}$. This large deviation shows that both feedbacks are highly related. As already mentioned in Chap. 2.3, a possible explanation for this correlation could be that both feedbacks are related to the deep convection in the tropical troposphere. A change in the deep convections scheme consequently influences the water vapour and the lapse rate feedback. When FW and BW PRP calculations are combined, the deviations of almost 20% between the sum and the combined feedback nearly cancel each other out.

For combined albedo and cloud feedbacks, the feedback parameter $\alpha_{(A+C)}$ deviates by about 6% for FW PRP and by about 24% for BW PRP calculation from the sum $\alpha_A+\alpha_C$. The combination of FW and BW PRP calculations results in a complete cancellation of the deviations. Clouds mask the surface albedo of snow and ice. For example, if an optically thick cloud is located above an ice cover, a melting of the ice will have no effect on the shortwave flux at TOA because the shortwave radiation cannot pass the optically thick cloud. Interestingly, the magnitude of the feedback parameters strongly differs for the FW and BW PRP calculations. The FW PRP calculation yields a 4 times higher sum of the feedbacks than the BW PRP calculation. Although, the absolute magnitude of the overlapping effect is the same for FW and BW PRP calculation (0.05 $\mathrm{Wm^{-2}K^{-1}}$), the relative magnitudes differ strikingly (6% for FW and 24% for BW PRP calculation).

Further, water vapour and clouds interact. Both FW and BW PRP calculations show a large difference between the sum and the combined feedback parameter of about 1.25 $\mathrm{Wm^{-2}K^{-1}}$. A possible explanation for the high correlation between the two feedback mechanism is that a change in the water vapour concentration also strongly affects the formation of clouds. Even this large overlapping effect totally vanish when FW and BW PRP calculations are combined.

Finally, the two strongest feedback mechanism are analysed. Surprisingly, the Planck and water vapour feedback interact very little. For the FW PRP calculation, the interaction accounts for only 14%, for the BW PRP calculation even less with 4%. Thus, the homogeneous change in tropospheric temperature profile does not influence the water vapour concentration and vice versa. Here, the separability of the two feedbacks is obvious.

Even though the feedback parameters for the FW and BW PRP calculations may differ substantially (e.g., the FW PRP calculation for the albedo-cloud-feedback is four times larger than for the BW PRP calculation), the magnitude of the difference between the sum and the combined feedbacks stays rather constant. Hence, the relative importance of the overlapping effects depends on the considered PRP calculations.

Further, it is interesting to note that the differences between the sum and the combination of the particular feedbacks for the FW and BW PRP calculation have opposite signs. Whenever one PRP calculation overestimates the feedbacks' sum compared to the combined feedbacks, the other PRP calculation underestimates the sum. The combination of FW and BW PRP calculation compensates this over- and underestimation. Thus, the (FW+BW) PRP calculation always reduces the difference between the overlapping

effects of the feedbacks. As a consequence the assumption of separable feedbacks is better justified, if the FW and BW PRP calculations are averaged.

4.5 Climate feedbacks under selected CO_2 driven climate change simulations

The variation of climate feedbacks under different strengths of radiative forcings is investigated in this section. As already mentioned in Chap. 3.2, three CO_2 driven simulations were performed by Dietmüller (2011) and are analysed hereafter: (a) an increase of atmospheric CO_2 concentration by 75 ppmv to a value of 442 ppmv, (b) a doubling, and (c) a quadrupling of the CO_2 concentration. The resulting instantaneous radiative forcing due to the different CO_2 increases are listed in Tab. 4.4. Dietmüller (2011) designed the 75 ppmv increase simulation to normalise the stratosphere adjusted radiative forcing to 1 Wm^{-2} for a later comparison with non-CO_2 forcing simulations with corresponding forcing strength. For this simulation, the instantaneous radiative forcing at TOA is 0.63 Wm^{-2}.

Experiment	CO_2 [ppmv]	RF_{inst} [Wm^{-2}]	λ_{inst} [K/Wm^{-2}]
(a) 442CO2	442	0.63 ± 0.001	1.12 ± 0.19
(b) 2xCO2	734	2.54 ± 0.003	1.09 ± 0.04
(c) 4xCO2	1468	5.70 ± 0.008	1.37 ± 0.03

Table 4.4: Instantaneous radiative forcing RF_{inst} and corresponding climate sensitivity parameter λ_{inst} including the standard deviations for the 442CO2 (increase of the CO_2 concentration by 75 ppmv), 2xCO2 (doubling of the CO_2 concentration), and 4xCO2 (quadrupling of the CO_2 concentration) simulations. Only the simulations without interactively coupled atmospheric chemistry (*nochem*) are considered.

Fig. 4.5 shows the corresponding feedback parameters and their standard deviations for these three simulation experiments. The FW, BW, and combined (FW+BW) PRP calculations are plotted. Since the variation of the individual feedback parameters should be compared, the range of the ordinate for all figures is the same and has a value of 5.0 $Wm^{-2}K^{-1}$. For the 442CO2 simulation, an ensemble of 28 years were evaluated. To calculate the feedback parameters of the 2xCO2 and 4xCO2 simulation, the means are formed over 24 and 17 years, respectively.

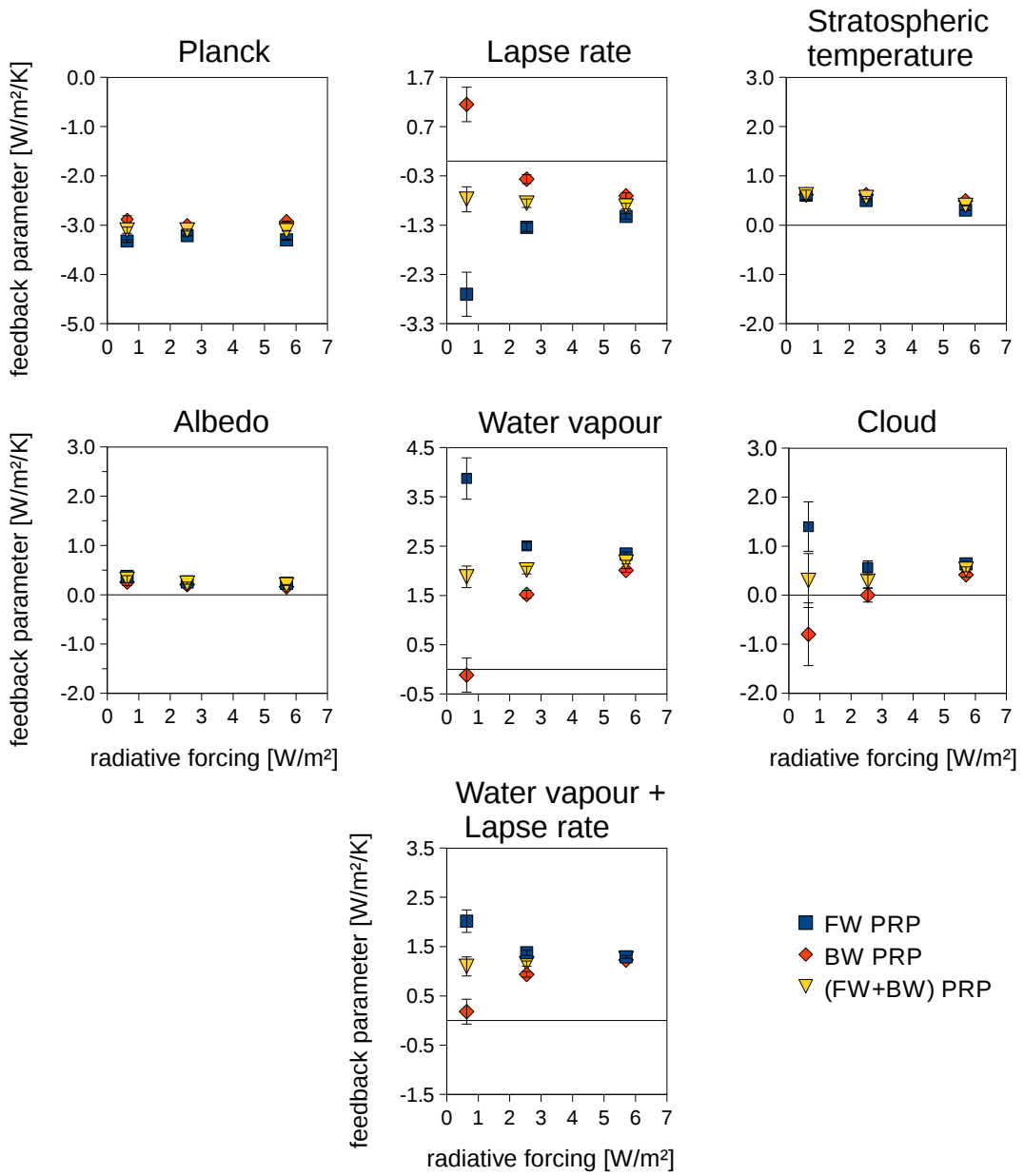

Figure 4.5: Feedback parameters of (a) 75 ppmv CO_2 increase (inducing an instantaneous forcing of 0.63 Wm^{-2}), (b) doubling of CO_2 (instantaneous forcing 2.54 Wm^{-2}), and (c) quadrupling of CO_2 (instantaneous forcing 5.70 Wm^{-2}) *nochem* simulations at TOA. The plots show the values for the FW, BW, and (FW+BW) PRP calculations. To be able to compare the variation of the feedback parameters, all plots show the same range of the ordinate. The error bars indicate one standard deviation.

Fig. 4.6 presents the zonal distributions of the various feedback parameters for all three radiative perturbation strengths. The zonal contribution of the feedback parameters are divided by the global mean surface temperature change. Thus, Fig. 4.6 indicates the latitude depended contributions to the global mean feedback parameter and not the local feedback parameters. Only the values of the (FW+BW) PRP calculation are shown. Note that the scale of the ordinate varies for each feedback parameter so that the effects of different perturbation strengths are highlighted.

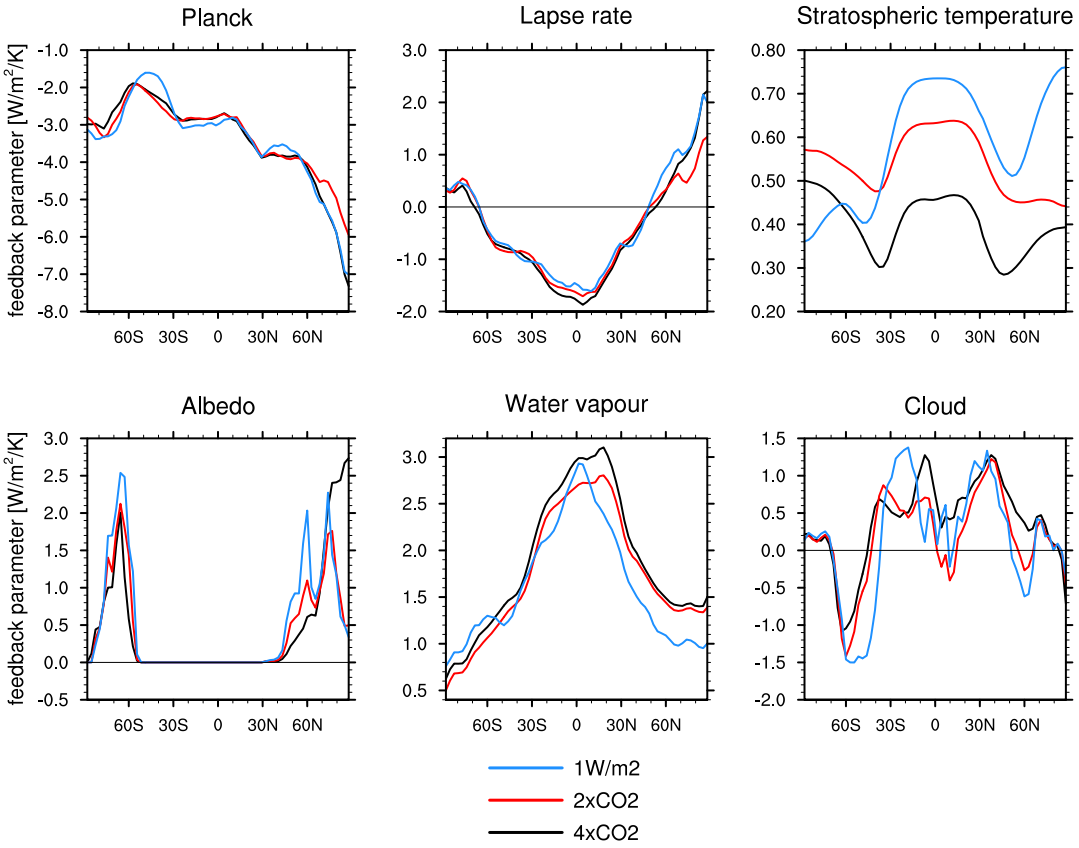

Figure 4.6: Zonal distributions of feedback parameters of (a) 75 ppmv CO_2 increase (442CO2 simulation), (b) doubling of CO_2 (2xCO2), and (c) quadrupling of CO_2 (4xCO2) *nochem* simulations. The plots show the values for the (FW+BW) PRP calculation. Note that the range of the ordinate varies for each feedback parameter. Unit: $Wm^{-2}K^{-1}$

At first, the feedback parameters of the combined (FW+BW) PRP calculation are considered. They show different behaviours for a varying strength of radiative forcing.

As radiative forcing increases, the Planck feedback parameter stays rather constant and the mean value in Fig. 4.5 varies only within 0.4%. Furthermore, the zonal distributions of the three radiative forcing strengths in Fig. 4.6 are very similar. Variations are only

found in the Northern latitudes which do no contribute substantially to the global mean value. This uniformity of the Planck feedback with the radiative forcing indicates that the surface and also atmospheric temperature rises linearly with an increase of the forcing.

With enhanced forcing, the lapse rate feedback parameter becomes more negative (by 18%). The trend is dominated by the negative contribution of the tropics where the upper troposphere heats stronger than the lower troposphere (see Fig. 4.6). This decrease of the tropical lapse rate becomes stronger the more the climate is perturbed, leading to an enhanced negative feedback. Southern latitudes do not contribute to the observed trend of the lapse rate feedback whereas the Northern latitudes show an irregular variation rather than a linear trend of the feedback parameter with increased forcing.

Due to increasing radiative forcing, the stratospheric temperature feedback parameter decreases by 30% from a global mean value of 0.54 to 0.38 $Wm^{-2}K^{-1}$. This indicates that the stratospheric temperature decrease (as shown in Fig. A.2) per unit forcing is weakened, the stronger the radiative forcing gets. The influence of the stratospheric temperature decrease seems to become less important as the perturbation increase. The zonal distributions in Fig. 4.6 for the three CO_2 driven simulations indicate a minimum at mid-latitudes and maximum at low and high latitudes. In the tropics as well as in the Northern polar latitudes, the stratospheric temperature feedback decreases considerably with increased forcing.

Although the surface albedo feedback parameter appears almost constant in Fig. 4.5, it still declines by about 30% when the CO_2 concentration is increased. In a warmer climate, less snow and ice can be found. Thus a rise in temperature in a warmer climate will have less effect on the snow and ice cover, the surface albedo feedback parameter decreases. This trend can be also seen in the zonal distribution of the surface albedo feedback in Fig. 4.6. Interestingly, the 4xCO2 simulation shows a large increase in the Arctic region north of 70°N. The Arctic sea ice does not seem to be strongly affected when the CO_2 concentration is increased by only 75 ppmv or if it is doubled. But the strong warming of a quadrupling of CO_2 induces substantial melting of the Arctic sea ice.

The water vapour feedback parameter rises with increasing radiative forcing from 1.68 to 2.09 $Wm^{-2}K^{-1}$. The tropics and the Northern latitudes in particular are responsible for this increase (Fig. 4.6). In these regions the uptake of water vapour in the air is not linear but augments with increased radiative forcing.

Further, the combined water vapour and lapse rate feedback is investigated in Fig. 4.5. In contrast to Colman and McAvaney (2009), who find no change of the feedback parameter with increasing radiative forcing, the feedback parameter in the EMAC model increases from a mean value of 0.99 to 1.21 $Wm^{-2}K^{-1}$. Besides, combining both feedbacks leads to a reduction of the standard deviation and of the difference between FW and BW PRP calculations. This further emphasises that the feedbacks are associated to the same physical process (see Chap. 2.3).

The cloud feedback shows no clear linear trend as the forcing increases. For the 442CO2 simulation the cloud feedback parameter has a value with corresponding 95% confidence interval of (0.31 ± 0.20) $Wm^{-2}K^{-1}$, for 2xCO2 simulation the feedback parameter is (0.28 ± 0.06) $Wm^{-2}K^{-1}$ and for 4xCO2, it is (0.51 ± 0.03) $Wm^{-2}K^{-1}$.

Fig. 4.7 presents the shortwave and longwave components of the cloud feedback. For different strength of forcing, the zonal distributions are very similar. The structure for the 2xCO2 and 4xCO2 simulations are even closer to each other than to the 442CO2 simulation, although their corresponding feedback parameters differ significantly. This suggests that already small changes in the magnitude of the local contributions strongly affect the global mean value. Further, the shortwave and longwave contribution are anticorrelated and offset each other. This causes a relatively small net cloud feedback (Colman et al., 2001).

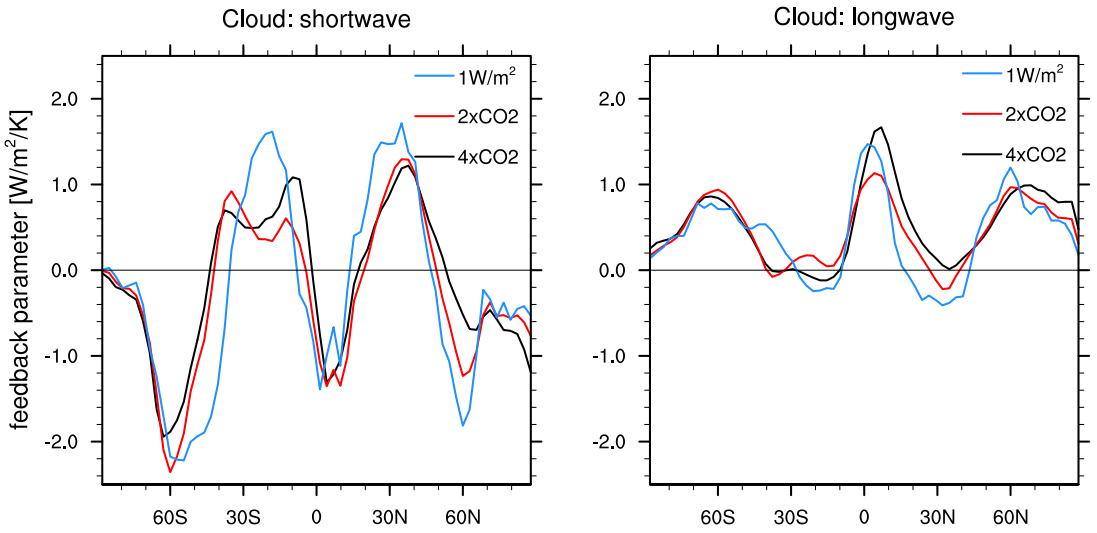

Figure 4.7: Zonal means of shortwave and longwave contribution to the cloud feedback parameters for *nochem* 442CO2, 2xCO2, and 4xCO2 simulations

Similar to Colman and McAvaney (2009), the shortwave component shows a shift of the strong negative minimum at 60°S towards the South pole as forcing rises. This might be associated to a displacement of the storm tracks and their corresponding cloud amount as pointed out by Colman and McAvaney (2009). Moreover, in the Northern Hemisphere a similar poleward shift and a decrease in magnitude of the minimum at 60°N is found. Apart from that, no specific trend with increasing radiative forcing is observed.

Further, the values of feedback parameters of the FW and BW PRP calculations are plotted in Fig. 4.5 to be able to compare between the two PRP calculations. For the surface albedo, Planck, and stratospheric temperature feedback, FW and BW PRP calculations correspond nicely. For the water vapour, the lapse rate, and the cloud feedback, the values for FW and BW PRP calculations show a strong dependence on the strength of forcing, which at the first glance are somewhat surprising. Especially for the 442CO2 simulation, which has the smallest forcing, the largest difference between the feedback parameters of the two PRP calculations occur. However, this behaviour vanishes when only the TOA flux changes calculated by the FW and BW PRP calculations are examined (see Fig. A.6). The difference between the flux changes of the two PRP calculations

for the 442CO2 simulation is small. The corresponding mean increase of surface temperature is 0.78 K (Tab. 3.1) and hence, smaller than 1 K. When the annual flux changes are divided by the surface temperature increases to calculate the feedback parameters, these small surface temperature increases blow up the difference between the feedback parameters of the FW and BW PRP calculations. However, to compare feedbacks under various strengths of the external radiative forcings and to identify potential differences, the feedback parameters and not the flux changes need to be compared. The latter results suggest that feedback calculations are much more sensitive to the background climate state if the radiative forcing is smaller. This result is somewhat counter-intuitive and can possibly only be explained if a special distinction is made between a slow feedback component and a fast feedback component (so-called "tropospheric adjustment", see Gregory and Webb (2008); Vial et al. (2013)) is made.

In particular, the water vapour feedback parameter in the BW PRP calculation is close to zero (-0.07 $\pm$ 0.32 $Wm^{-2}K^{-1}$). Although generally assumed to be the largest positive feedback (as confirmed for the standard cases of a doubling or quadrupling of CO_2 concentration), in this case of a small perturbation, the BW PRP calculation yields a water vapour feedback which is even smaller than the albedo feedback. A closer look at the basic parameter changes revealed that for the 442CO2 simulation, the water vapour concentration does not increase all over the atmosphere as expected for a global warming. Small but numerous regions hold a decrease of the water vapour concentration. These water vapour increases and decreases in the atmosphere cause positive and negative flux changes at TOA for the BW PRP calculation. When globally averaged, the positive and negative flux cancel each other out and result in a value close to zero. Whereas for the FW PRP calculation, the water vapour increases and decreases result only in a positive flux changes at TOA and hence in a strong positive value of (3.44 $\pm$ 0.32) $Wm^{-2}K^{-1}$.

Further, the lapse rate feedback of the BW PRP calculation for the 442CO2 simulation has an opposite sign than of the FW PRP calculation. Here, the behaviour of the extratropics is the dominating factor. In contrast to the expected positive values in the extratropics (as shown in Fig. 4.1 for the 2xCO2 simulation), the extratropics have only negative values in the FW PRP calculation for the 442CO2 simulation. Whereas for the BW PRP calculation, the values in the extratropics are strongly positive (as expected), thus resulting in an positive global averaged value. In this case the extratropics dominate the sign of the feedback parameter and also determine whether the feedback amplifies or dampens to the initial perturbation.

To be able to understand the unusual features that show up under a smaller radiative forcing, a differentiation between slow and fast feedback components could be revealing. Since this was not possible in this master thesis, further investigations beyond this thesis are needed.

5 Discussion

In this thesis, radiative feedback processes such as the Planck, lapse rate, stratospheric temperature, water vapour, albedo, and cloud feedbacks are investigated. The basic data are taken from several simulations forced by various increases of atmospheric CO_2 concentration. To determine the feedback parameters, the "Partial Radiative Perturbation"-method is used. This work investigates the strengths and weaknesses of the PRP-method. The FW or the BW PRP calculation may provide very different results for the same feedback parameter. For the Planck feedback, the FW and BW PRP calculation differ only by 7% for the 2xCO2 simulation experiment, but for all other feedbacks the variation is at least 20%. In particular, for a small CO_2 radiative forcing, the greatest variation between the two PRP calculations can be found for the lapse rate, the water vapour, and the cloud feedback. This indicates that the determination of feedback parameters is very sensitive to small perturbations depending on whether the reference or the climate change experiment is considered. For large perturbations, the feedback calculations are robust and do not strongly depend on the chosen climate state. The stronger the applied perturbation gets, the better FW and BW PRP calculation seem to agree. Block and Mauritsen (2013) investigates feedbacks under a quadrupling of CO_2 by means of radiative kernels. The radiative kernels for the reference and the climate change simulations are calculated by perturbing each climate state with a unit change. They also found that feedbacks in the reference and in the climate change experiment behave differently. Thus, this study confirms that the climate response depends on the considered climate state.

Feedback analyses of equilibrium climate change simulations are based on certain key assumptions such as reestablishment of the radiation balance, i.e. the full set of radiative feedbacks balances the radiative forcing at TOA, and negligible overlaps between individual feedbacks. When only the results for either FW or BW PRP calculation are considered, the reestablishment of the radiation balance at TOA is masked, as a large residuum shows up. Furthermore, the split-up of the total climate feedback into individual feedbacks appears not to be justified (Chap. 4.4). The sum of the individual feedbacks does not correspond to the total feedback. Overlapping effects between the feedbacks occur and the assumption of the additivity for these feedbacks fails. Only in case of the temperature related feedbacks, the separability is always evident; for other feedbacks, their separation has to be regarded with considerable caution when just the single PRP calculation is considered. The error made can account for up to 80% of the feedback parameter. The water vapour and lapse rate feedback in particular should be considered together, which is already done often (e.g. Bony et al. (2006)). The separability of the water vapour and cloud feedback seems to be also questionable for the single FW or BW PRP calculations (Chap. 4.4).

Only when FW and BW PRP calculations are combined, these overlapping effects cancel out. The sum of the feedbacks equals the total feedback and the assumption of the additivity that presents the basic principle of the PRP-method becomes justified. Furthermore, the radiation balance at TOA is restored when results of the combined (FW+BW) PRP calculation are considered. Consequently, for a useful feedback analysis, only the combination of the FW and BW PRP calculation should be applied to provide results which are suitable for a sensible physical interpretation.

For the standard case of CO_2 doubling simulations, the results of this work are in good agreement with other studies (Soden and Held, 2006; Bony et al., 2006; Klocke et al., 2013). To quantify the feedback processes as reliable as possible, an ensemble of 24 simulation years is taken into account. This is necessary to reduce the high statistical noise of several feedbacks such as the water vapour and the cloud feedback. In contrast, Klocke et al. (2013) just considered 6 years in their feedback analysis, which, for example, has resulted in a standard deviation for the cloud feedback that is twice as high than found in this work. In particular for the cloud feedback, a large ensemble of years reduces the standard deviation of the feedback parameter and thus increases the certainty of the value.

When small radiative forcings are considered, the interannual variability of radiative feedback parameters around their multi-year mean increases considerably. For the 442CO2 simulation experiment, the standard deviations are up to 5 times higher than for the 2xCO2 simulation. Although a larger ensemble of evaluated years for the 442CO2 simulation than for the 2xCO2 experiment is considered, the standard deviations could not be reduced compared to the 2xCO2 experiment. The climate state varies substantially from year to year. Here, the applied perturbation is very small and thus it is difficult to extract the mean effect of the perturbation from the high interannual variability of the climate with a sufficiently high accuracy to be able to compare with other simulations. The feedback parameters of the 442CO2 simulation experiment show a larger 95% confidence interval, making it more problematic to interpret these results physically.

This work introduces the stratospheric temperature feedback as a separate part of the temperature feedback. The reason why the stratospheric temperature change can be regarded separately is that it develops independly from the tropospheric temperature feedbacks, namely Planck and lapse rate feedbacks (Chap. 2.3). For a doubling of the atmospheric CO_2 concentration, the stratospheric temperature feedback results in a small value of 0.56 $Wm^{-2}K^{-1}$ which corresponds to a flux change of 1.55 Wm^{-2} at TOA (Chap. 4.1). Colman (2002, 2003) also considers the stratospheric temperature change for the case of doubling CO_2. He reports an effect of 1.5 to 2.2 Wm^{-2} due to stratospheric cooling. The value of 1.55 Wm^{-2} found in this work is in good agreement with the reported range. Colman (2002, 2003) does not regard the temperature change in the stratosphere as a separate feedback. Instead, he subtracted the flux change due to stratospheric temperature change from the lapse rate feedback.

If the stratosphere adjusted radiative forcing is considered as part of the forcing and feedback balance, the stratospheric temperature change is not regarded as a separate

feedback but as part of the forcing. However, this work uses the instantaneous radiative forcing for this purpose, as it is consistent with the calculation of the radiative feedback parameters. To estimate the stratosphere adjusted radiative forcing from instantaneous values, the flux change induced by the stratospheric temperature feedback of 1.55 Wm^{-2} is added to the instantaneous radiative forcing of 2.54 Wm^{-2} (Tab. 4.4). This results in a stratosphere adjusted radiative forcing of 4.09 Wm^{-2} which is in good agreement with the value of 4.13 Wm^{-2} calculated by Dietmüller (2011) (Tab. 3.1). Thus, instead of comparing only the instantaneous radiative forcing and the instantaneous feedbacks ($\alpha_{pla}, \alpha_{LR}, \alpha_{str}, \alpha_q, \alpha_A, \alpha_C$), it would be also justified to compare the stratosphere adjusted radiative forcing and the instantaneous feedbacks without the stratospheric temperature feedback ($\alpha_{pla}, \alpha_{LR}, \alpha_q, \alpha_A, \alpha_C$) as methodically has been done by Klocke et al. (2013). However, they do not include stratospheric temperature changes that are not induced by the CO_2 increase but by changes of other climate variables such as water vapour or cloud properties in their radiation balance. This could explain their larger residual term of 9% compared to the value of 5% found in this work.

After the climate is perturbed, it will reach a new equilibrium state where the feedbacks balances the perturbation. The net radiation balance at TOA should be restored. Nevertheless, for the 2xCO2 simulation an imbalance of 0.05 $Wm^{-2}K^{-1}$ remains which means less than 5% of the radiative forcing. Often, the residual terms are neglected when feedbacks are analysed. Vial et al. (2013) determined the feedbacks of 11 models, calculated by the radiative kernel method. They further compared the residual terms for these models and found noteworthy variability. Only 6 models show a residual term of less than 10%. For some models, the residual term reaches as high as 120%. It is questionable if the separation of feedbacks is justified if models present such a high residual term.

The residual term found in this work is small compared to other studies (Klocke et al., 2013; Shell et al., 2008; Vial et al., 2013). Hence, the applied method is very suitable to describe the restoration of the radiative balance by the developing radiative feedbacks. The theoretically assumed closure between the radiation forcing and the sum of the radiative feedbacks is well represented, which confirms that the separability of the feedbacks is justified.

The online calculated fluxes by Dietmüller (2011) also show an imbalance at TOA, possibly due to a constant flux correction for all simulations. The imbalance increases by 0.20 Wm^{-2} when the CO_2 concentrations is doubled. Hence, the offline flux calculations performed in this work should also show this imbalance. The residual term of 0.05 $Wm^{-2}K^{-1}$ corresponds to a flux change of 0.15 Wm^{-2} and thus has a similar magnitude as the imbalance found in the original data of Dietmüller (2011). This could be a possible explanation for the source of the residual term between the radiative forcing and the sum of the feedbacks.

All feedbacks accounted together counteract the radiative forcing. According to Eq. 5.1 the sum of the feedback parameters α is hence the negative reciprocal of the climate sensitivity parameter λ.

$$\alpha = \sum_x \alpha_x = -\frac{RF}{\Delta T_S} = -\frac{1}{\lambda} \tag{5.1}$$

In this sense, variations in the sum of the feedback α can provide information about the behaviour of the climate sensitivity. The sum of the feedback parameters and the reciprocal of the climate sensitivity parameter for the CO_2 driven simulations are compared in Tab. 5.1. The climate sensitivity parameter corresponds to the instantaneous radiative forcing (Tab. 4.4) and thus differs from the values reported by Dietmüller (2011) that are calculated by the stratosphere adjusted radiative forcing method (Tab. 3.1). However, the instantaneous climate sensitivity parameters show the same behaviour as the stratosphere adjusted ones: For the 442CO2 and 2xCO2 simulation, due to internal variations, the climate sensitivities (Tab. 5.1) cannot be distinguished, but the 4xCO2 simulation presents a notably higher climate sensitivity parameter or a significantly smaller reciprocal climate sensitivity parameter as shown in Tab. 5.1. The sum of the feedbacks α for the 442CO2 simulations presents such a high internal variability that a statistically significant difference from the 2xCO2 and 4xCO2 simulations cannot be established. Hence, the feedback analysis for the 442CO2 simulation is not suitable to explain differences in the climate sensitivity. To identify the reasons for the varying climate sensitivity parameter, the feedback analysis in the following is concentrated on the 2xCO2 and 4xCO2 simulations where the mean values for the sum of the feedbacks can be significantly distinguished.

Experiment	λ^{-1}	α
	[$Wm^{-2}K^{-1}$]	[$Wm^{-2}K^{-1}$]
(a) 442CO2	0.92 ± 0.06	-0.77 ± 0.23
(b) 2xCO2	0.92 ± 0.02	-0.87 ± 0.07
(c) 4xCO2	0.73 ± 0.01	-0.73 ± 0.03

Table 5.1: Reciprocal climate sensitivity parameter λ^{-1} (corresponding to the instantaneous radiative forcing, Tab. 4.4), the total feedback parameter α, and their corresponding 95% confidence intervals for CO_2 driven climate simulations 442CO2, 2xCO2 and 4xCO2. Considered are the *nochem* simulations. Unit: $Wm^{-2}K^{-1}$

When the atmospheric CO_2 concentration is quadrupled, the climate sensitivity parameter increases by 26% (Tab. 4.4) meaning that the reciprocal climate sensitivity drops by about 0.19 $Wm^{-2}K^{-1}$ (Tab. 5.1). The absolute value of the feedback parameter α also decreases by 0.14 $Wm^{-2}K^{-1}$, which indicates that a reduction of the feedback processes induces the decrease of the reciprocal climate sensitivity parameter or the increase of the climate sensitivity parameter.

The decline of the absolute value of the feedback parameter α can be explained by the behaviour of the individual feedbacks due to different strengths of forcings. Fig. 5.1

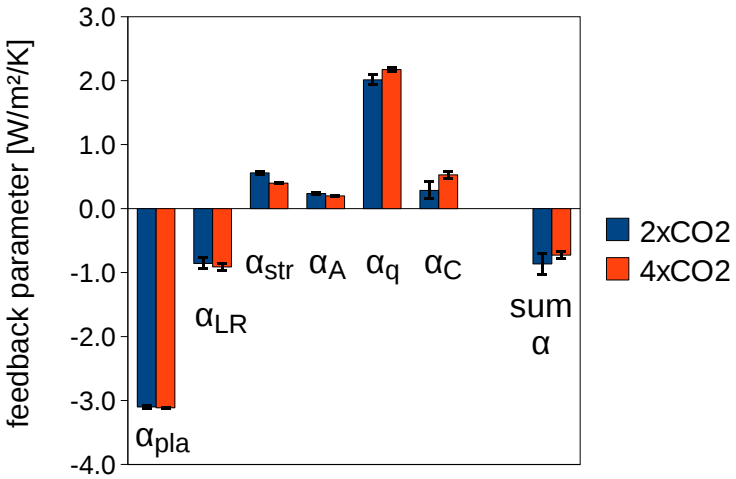

Figure 5.1: Comparison of the Planck (α_{pla}), lapse rate (α_{LR}), stratospheric temperature (α_{str}), albedo (α_A), water vapour (α_q), and cloud (α_C) feedback parameters for *nochem* 2xCO2 and 4xCO4 simulation experiments. The values of the (FW+BW) PRP calculation are displayed. Error bars indicate one standard deviation.

compares the various feedback parameters for the 2xCO2 and 4xCO2 simulations to illustrate the variation of the feedback parameters. The exact values are given in Tab. 4.1 and Tab. A.2. As already mentioned in Chap. 4.5, and as again shown in Fig. 5.1, the Planck feedback varies so little over the investigated range of forcing that it may not be accounted for the deviation of the climate sensitivity parameters. The lapse rate feedback strengthens only by 0.05 $Wm^{-2}K^{-1}$ and the albedo feedback weakens slightly (0.03 $Wm^{-2}K^{-1}$) when the CO_2 concentration is quadrupled. This suggets that the lapse rate and the surface albedo feedback are not responsible for the varying climate sensitivity. In contrast, the stratospheric temperature feedback drops strongly by about 0.16 $Wm^{-2}K^{-1}$ which is nearly canceled out by the water vapour feedback. The latter increases by 0.17 $Wm^{-2}K^{-1}$. Although this rise corresponds only to 8% of the feedback's magnitude, it is not negligible. The cloud feedback varies the most. It increases from a value of 0.29 $Wm^{-2}K^{-1}$ for the 2xCO2 simulation to a value of 0.53 $Wm^{-2}K^{-1}$ for the 4xCO2 simulation. This strong increase of the cloud feedback (0.24 $Wm^{-2}K^{-1}$) increases the sum of the feedback α which corresponds to a decrease of the absolute value of the feedbacks' sum. Hence, the effect of the total feedback is weakened when the CO_2 is quadrubled compare to a doubling of CO_2.

Consequently, the interplay of the stratospheric temperature, the water vapour, and cloud feedback determines the behaviour of the total feedback parameter and therefore, of the climate sensitivity parameter for CO_2 driven climate change simulations. To understand how climate will change, it is in particular important to further investigate

these three feedback processes.

For CO_2 driven climate change simulations with large radiative forcings, it was possible to identify the feedback processes which are responsible for the variation in the climate sensitivity parameter. However, as mentioned earlier, the diversity of the climate sensitivity parameter does not only depend on the strengths but also (or even more) on different types of radiative forcings. Dietmüller (2011) also performed climate change simulations driven by an increase of NO_x and CO emissions. This caused a relatively small radiative forcing of 1 Wm^{-2} which is comparable to the magnitude of the radiative forcing for the 442CO2 simulation experiment. However, as shown above, the radiative forcing for the 442CO2 experiment is very small and thus the interannual variability is too high to identify the feedback processes which are responsible for differences in the climate sensitivity parameter. Similar, the NO_x/CO emission increase simulations, which also own a small radiative forcing, show a high interannual variability (Dietmüller, 2011) and, thus, also for these simulation experiments, it is questionable, if a feedback analysis will offer valuable indications to the reasons for the variations in climate sensitivity.

It is also worthwhile to recall that for climate change simulations which are perturbed by non-CO_2 radiative forcings, stratosphere adjusted radiative forcings and feedbacks better describe climate change (Hansen et al., 1997). Hence, for the evaluation of the NO_x/CO driven simulations, the examination of the stratosphere adjusted radiative forcings and feedbacks would be preferable. Therefore, the integration of the stratospheric temperature adjustment to the radiation transfer model is the next step to be done.

A Appendix

A.1 Input parameters for CO_2 doubling experiment

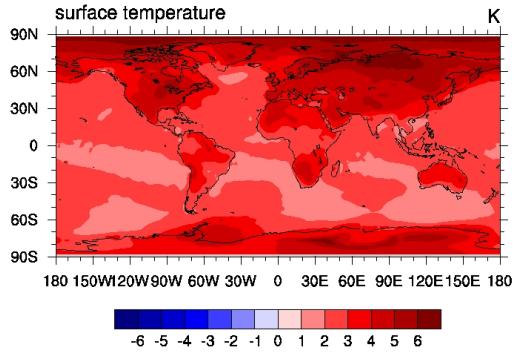

Figure A.1: Increase of surface temperature in K due to a doubling of the atmospheric CO_2 concentration. (Dietmüller, 2011)

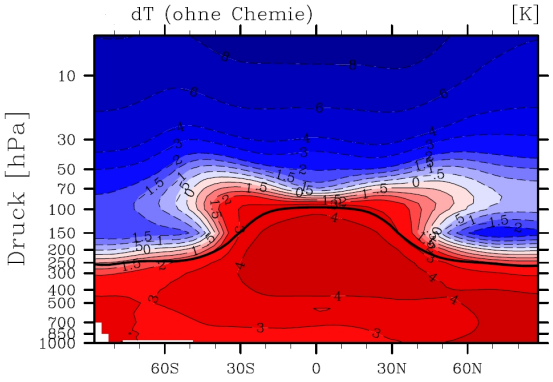

Figure A.2: Zonal mean of the temperature change in K due to a doubling of the atmospheric CO_2 concentration. The bold line represents the tropopause. (Dietmüller, 2011)

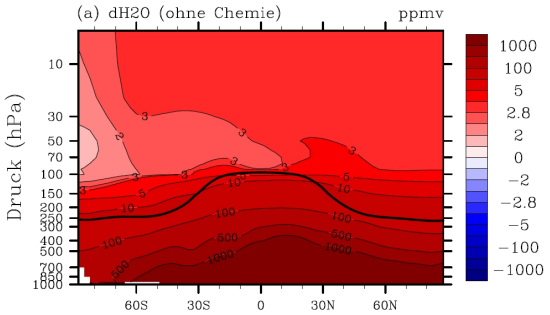

Figure A.3: Zonal mean of the absolute water vapour change in ppmv due to a doubling of the atmospheric CO_2 concentration. The bold line represents the tropopause. (Dietmüller, 2011)

A.2 Supplementary results of CO_2 doubling experiment

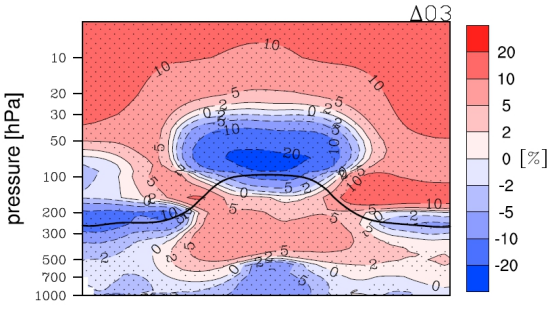

Figure A.4: Zonal mean of the ozone percentage change due to a doubling of the atmospheric CO_2 concentration. The bold line represents the tropopause. Stippling indicates statistical on a 95% confidence level. (Dietmüller et al., 2014)

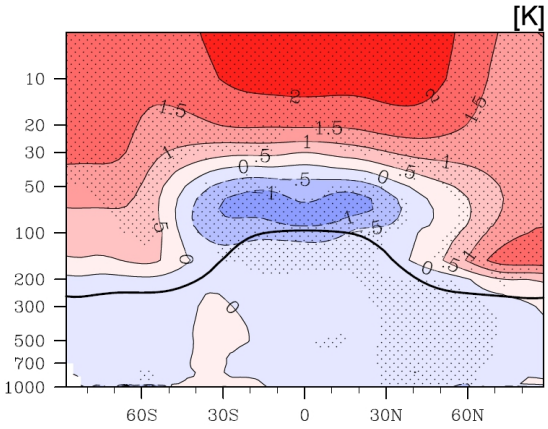

Figure A.5: Zonal mean of the absolute temperature change in K due to interactively coupled atmospheric chemistry for doubling of the atmospheric CO_2 concentration. The bold line represents the tropopause. Stippling indicates statistical on a 95% confidence level. (Dietmüller et al., 2014)

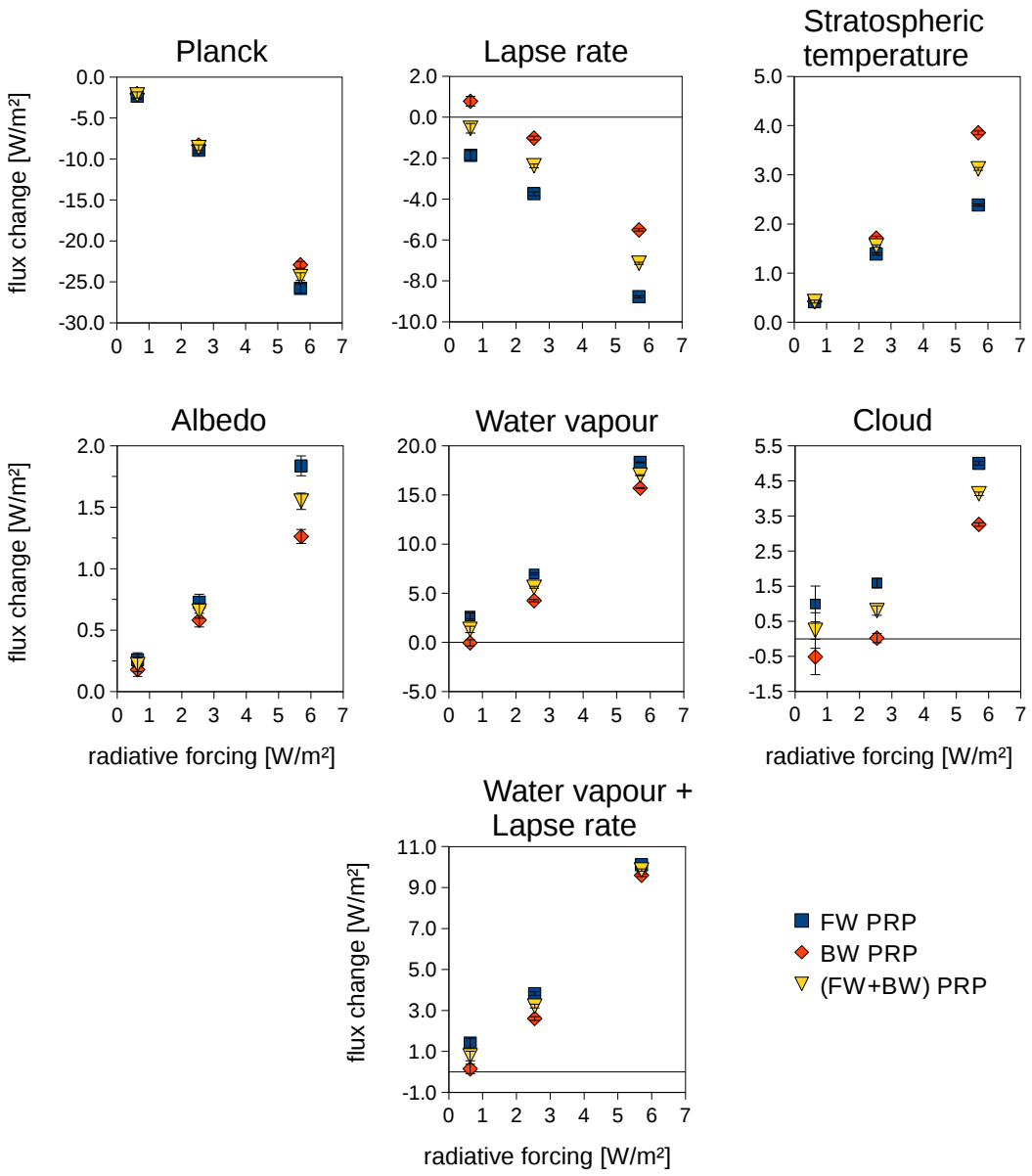

Figure A.6: Flux changes in Wm^{-2} of (a) 75 ppmv CO_2 increase (inducing an instantaneous forcing of 0.63 Wm^{-2}), (b) doubling of CO_2 (instantaneous forcing 2.54 Wm^{-2}), and (c) quadrupling of CO_2 (instantaneous forcing 5.70 Wm^{-2}) *nochem* simulations. The plots show the values for the FW, the BW, and the (FW+BW) PRP calculation. For each plot, the range of the ordinate vary. The error bars indicate one standard deviation.

A.3 Results of 442CO2 simulation

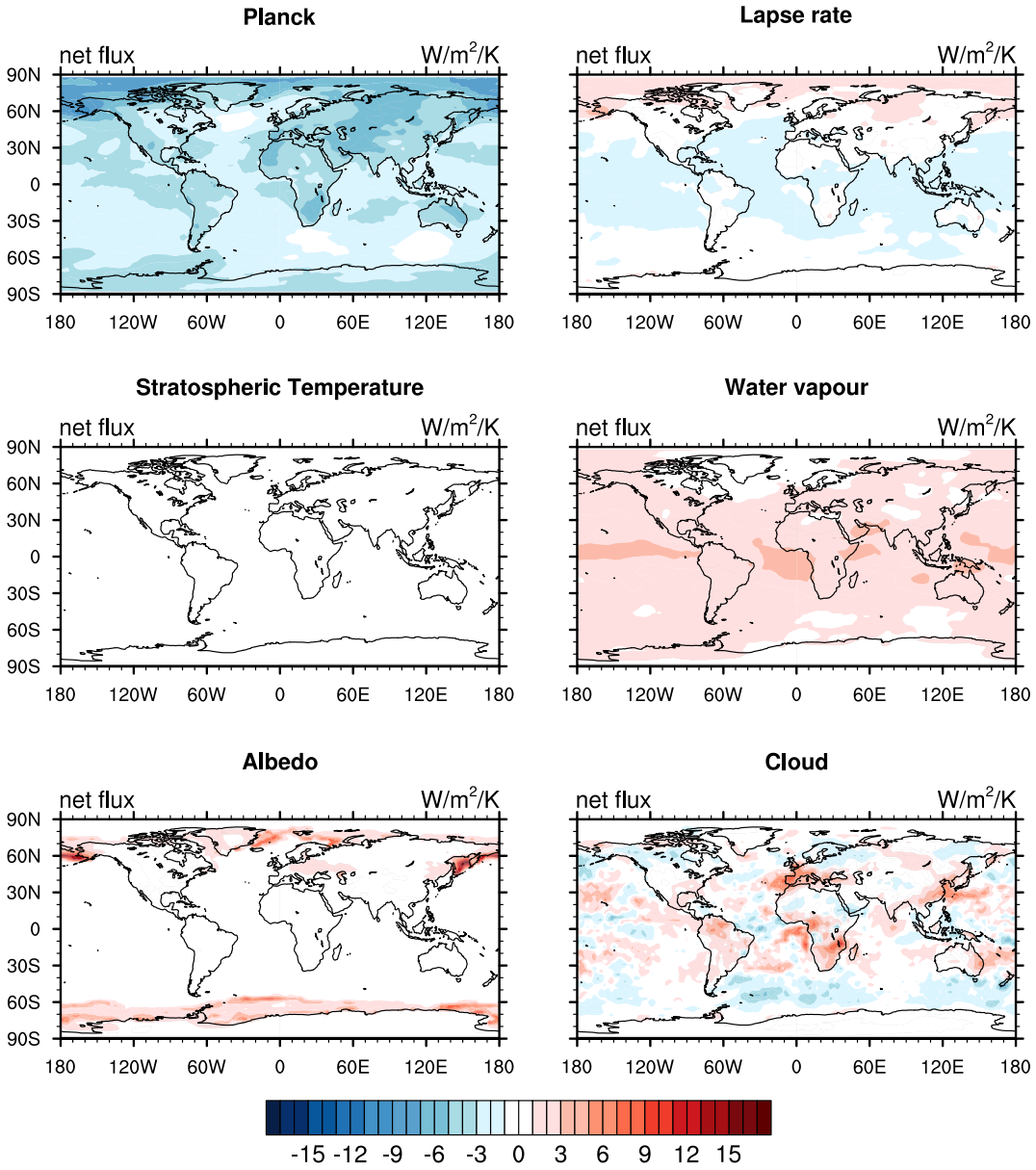

Figure A.7: Global distribution of net Planck, lapse rate, stratospheric temperature, water vapour, albedo, and cloud feedback parameters for an increase of CO_2 by 75 ppmv to a value of 442 ppmv (*nochem* 442CO2 simulation) at TOA for the combined (FW+BW) PRP calculation. Positive values denote an increased downward radiation. Unit: $Wm^{-2}K^{-1}$

α_x	PRP calculation	SW	SW std	LW	LW std	net	net std
α_{pla}	FW PRP	0	0	-3.32	0.07	-3.32	0.07
	BW PRP	0	0	-2.88	0.07	-2.88	0.07
	(FW+BW) PRP	0	0	-3.10	0.06	-3.10	0.06
α_{LR}	FW PRP	0	0	-2.70	0.45	-2.70	0.45
	BW PRP	0	0	1.15	0.35	1.15	0.35
	(FW+BW) PRP	0	0	-0.78	0.25	-0.78	0.25
α_{str}	FW PRP	0	0	0.61	0.10	0.61	0.10
	BW PRP	0	0	0.62	0.10	0.62	0.10
	(FW+BW) PRP	0	0	0.61	0.10	0.61	0.10
α_A	FW PRP	0.37	0.08	0	0	0.37	0.08
	BW PRP	0.27	0.07	0	0	0.26	0.07
	(FW+BW) PRP	0.31	0.08	0	0	0.31	0.08
α_q	FW PRP	0.37	0.04	3.50	0.39	3.87	0.42
	BW PRP	0.29	0.04	0.41	0.34	0.12	0.35
	(FW+BW) PRP	0.33	0.04	1.54	0.19	1.88	0.22
α_C	FW PRP	0.02	0.57	1.38	0.27	1.40	0.50
	BW PRP	-0.12	0.58	0.67	0.26	0.80	0.64
	(FW+BW) PRP	-0.05	0.57	0.36	0.21	0.30	0.55

Table A.1: Shortwave (SW), longwave (LW), and net feedback parameters and corresponding standard deviation (std) for an increase of CO_2 by 75 ppmv to a value of 442 ppmv (*nochem* 442CO2 simulation). Values are given for the FW, BW, and the combined (FW+BW) PRP calculations. Unit: $Wm^{-2}K^{-1}$

A.4 Results of 4xCO2 simulation

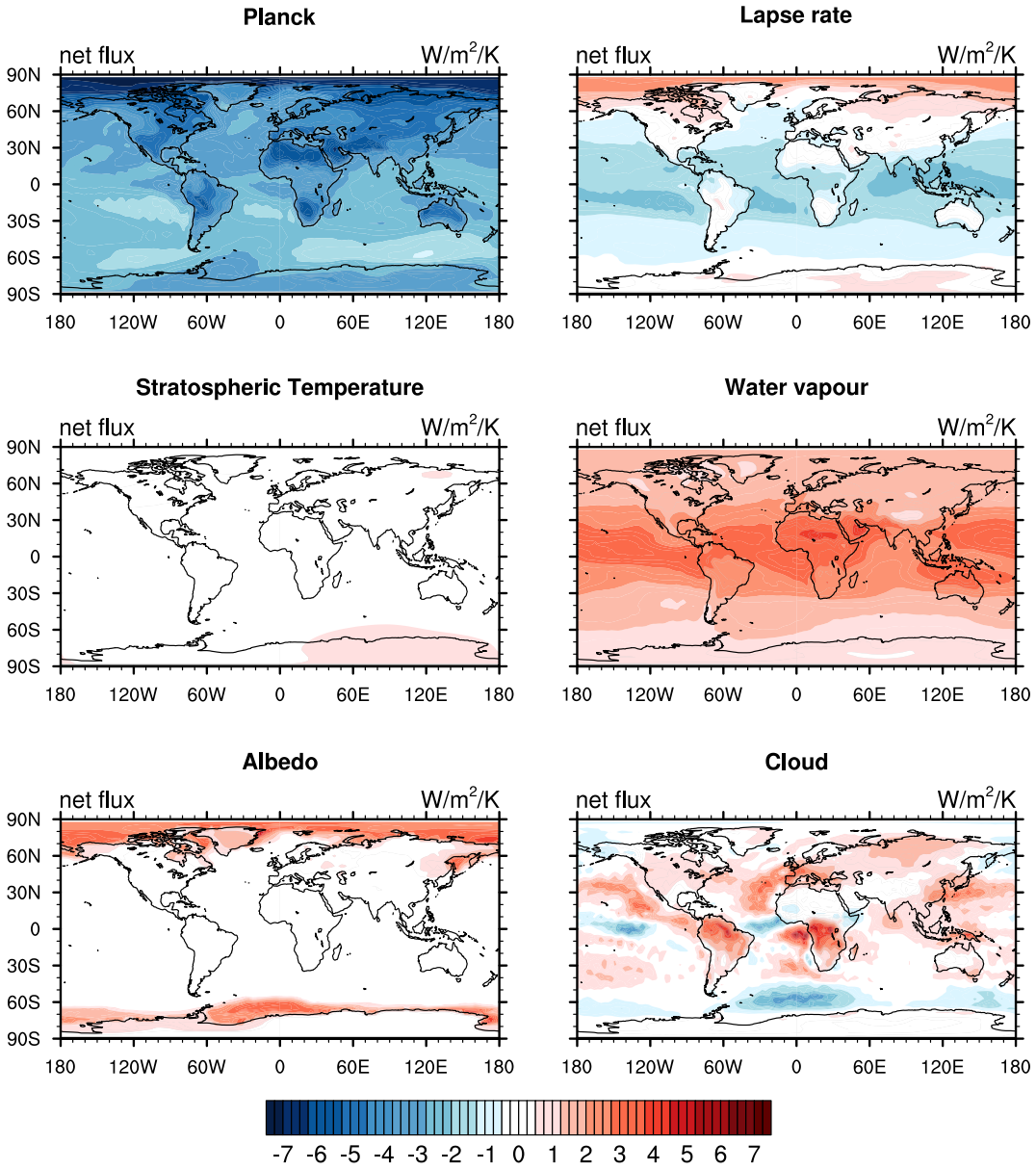

Figure A.8: Global distribution of net Planck, lapse rate, stratospheric temperature, water vapour, albedo, and cloud feedback parameters for CO_2 quadrupling (*nochem* 4xCO2 simulation) at TOA for the combined (FW+BW) PRP calculation. Positive values denote an increased downward radiation. Unit: $Wm^{-2}K^{-1}$

α_x	PRP calculation	SW	SW std	LW	LW std	net	net std
α_{pla}	FW PRP	0	0	-3.30	0.02	-3.30	0.02
	BW PRP	0	0	-2.93	0.01	-2.93	0.01
	(FW+BW) PRP	0	0	-3.11	0.01	-3.11	0.01
α_{LR}	FW PRP	0	0	-1.12	0.05	-1.12	0.05
	BW PRP	0	0	-0.70	0.06	-0.70	0.06
	(FW+BW) PRP	0	0	-0.91	0.06	-0.91	0.06
α_{str}	FW PRP	0	0	0.31	0.01	0.31	0.01
	BW PRP	0	0	0.49	0.01	0.49	0.01
	(FW+BW) PRP	0	0	0.40	0.01	0.40	0.01
α_A	FW PRP	0.24	0.01	0	0	0.24	0.01
	BW PRP	0.16	0.01	0	0	0.16	0.01
	(FW+BW) PRP	0.20	0.01	0	0	0.20	0.01
α_q	FW PRP	0.38	0.01	1.96	0.04	2.34	0.04
	BW PRP	0.36	0.04	1.65	0.05	2.01	0.04
	(FW+BW) PRP	0.37	0.02	1.81	0.04	2.18	0.04
α_C	FW PRP	0.09	0.04	0.55	0.04	0.64	0.05
	BW PRP	0.01	0.04	0.41	0.04	0.42	0.05
	(FW+BW) PRP	0.05	0.04	0.48	0.04	0.53	0.05

Table A.2: Shortwave (SW), longwave (LW), and net feedback parameters and corresponding standard deviation (std) for a quadrupling of CO_2 concentration (*nochem* 4xCO2 simulation). Values are given for the FW, BW, and the combined (FW+BW) PRP calculation. Unit: $Wm^{-2}K^{-1}$

Bibliography

Aires, F. and Rossow, W. B. Inferring instantaneous, multivariate and nonlinear sensitivities for the analysis of feedback processes in a dynamical system: Lorenz model case-study. *Q. J. R. Meteorol. Soc.*, 129:239–275, 2003.

Berntsen, T., Fuglestvedt, J., Joshi, M., Shine, K., Stuber, N., Ponater, M., Sausen, R., Hauglustaine, D., and Li, L. Response of climate to regional emissions of ozone precursors: sensitivities and warming potentials. *Tellus*, 57B:283–304, 2005.

Block, K. and Mauritsen, T. Forcing and feedback in the MPI-ESM-LR coupled model under abruptly quadrupled CO_2. *J. Adv. Model. Earth Syst.*, 5:679–691, 2013.

Bony, S., Colman, R., Kattsov, V. M., Allan, R. P., Bretherton, C. S., Dufresne, J.-L., Hall, A., Hallegate, S., Holland, M. M., Ingram, W., Randall, D. A., Soden, B. J., Tselioudis, G., and Webb, M. J. How well do we understand and evaluate climate change feedback processes? *J. Climate*, 19:3445–3482, 2006.

Cess, R. D., Potter, G. L., Blanchet, J. P., Boer, G. J., Del Genio, A. D., Déqué, M., Dymnikov, V., Galin, V., Gates, W., Ghan, S. J., Kiehl, J. T., Lacis, A. A., Le Treut, H., Li, Z.-X., Liang, X.-Z., McAvaney, B. J., Meleshko, V. P., Mitchell, J. F. B., Morcrette, J.-J., Randall, D. A., Rikus, L., Roeckner, E., Royer, J. F., Schlese, U., Sheinin, D. A., Slingo, A., Sokolov, A. P., Taylor, K. E., Washington, W. M., Wetherald, R. T., Yagai, . I, and Zhang, M.-H. Intercomparison and interpretation of climate feedbacks processes in 19 atmospheric general circulation models. *J. Geophys. Res.*, 95(D10):16,601–16,615, 1990.

Colman, R. On the vertical extent of atmospheric feedbacks. *Climate Dyn.*, 17:391–405, 2001.

Colman, R. Geographical contributions to global climate sensitivity in a general circulation model. *Global Planet. Change*, 32:211–243, 2002.

Colman, R. A comparison of climate feedbacks in general circulation models. *Climate Dyn.*, 20:865–873, 2003.

Colman, R., Fraser, J., and Rotstayn, L. Climate feedbacks in a general circulation model incorporating prognostic clouds. *Climate Dyn.*, 18:103–122, 2001.

Colman, R. and McAvaney, B. Climate feedbacks under a very broad range of forcing. *Geophys. Res. Lett.*, 36:L01702, 2009.

Colman, R. A. and McAvaney, B. J. A study of general circulation model climate feedbacks determined from perturbed sea surface temperature experiments. *J. Geophys. Res.*, 102:19,383–19,402, 1997.

Dietmüller, S. *Relative Bedeutung chemischer und physikalischer Rükkopplungen in Klimasensitivitätsstudien mit dem Klima-Chemie-Modellsystem EMAC/MLO*. PhD thesis, Ludwig-Maximilians-Universität München, DLR-Forschungsbericht 2011-19, Deutschen Zentrum für Luft- und Raumfahrt, Germany, 2011. ISSN 1434-8454, pp. 124.

Dietmüller, S., Ponater, M., and Sausen, R. Interactive ozone induces a negative feedback in CO2 driven climate change simulations. *J. Geophys. Res.*, 119:1796–1805, 2014.

Gregory, J. and Webb, M. Tropospheric Adjustment Induces a Cloud Component in CO_2 Forcing. *J. Climate*, 21:58–71, 2008.

Hansen, J., Sato, M., and Ruedy, R. Radiative forcing and climate response. *J. Geophys. Res.*, 102:6831–6864, 1997.

Hansen, J., Sato, M., Ruedy, R., Nazarenko, L., Lacis, A., Schmidt, G. A., Russell, G., Aleinov, I., Bauer, M., Bauer, S., Bell, N., Cairns, B., Canuto, V., Chandler, M., Cheng, Y., Del Genio, A., Faluvegi, G., Fleming, E., Friend, A., Hall, T., Jackman, C., Kelley, M., Kiang, N., Koch, D., Lean, J., Lerner, J., Lo, K., Menon, S., Miller, R., Minnis, P., Novakov, T., Oinas, V., Perlwitz, J., Perlwitz, J., Rind, D., Romanou, A., Shindell, D., Stone, P., Sun, S., Tausnev, N., Thresher, D., Wielicki, B., Wong, T., Yao, M., and Zhang, S. Efficacy of climate forcings. *J. Geophys. Res.*, 110:D18104, 2005.

Held, I. M. and Soden, B. J. Water vapour feedback and global warming. *Annu. Rev. Energy Environ.*, 25:441–475, 2000.

IPCC, 2007. *Climate Change 2007: The Physical Science Basis. Contribution of Working Group I to the Fourth Assessment Report of the Intergovernmental Panel on Climate Change*. Solomon, S., Qin, D., Manning, M., Chen, Z., Marquis, M., Averyt, K.B., Tignor, M. and Miller, H.L. (eds.). Cambridge University Press, Cambridge, United Kingdom and New York, NY, USA. 996 pp.

IPCC, 2013. *Climate Change 2013 - The Physical Science Basis:Working Group I Contribution to the Fifth Assessment report of the Intergovernmental Panel on Climate Change*. Stocker, T.F., Qin, D., Plattner, G.-K., Tignor, M., Allen, S.K., Boschung, J., Nauels, A., Xia, Y., Bex, V. and Midgley, P.M. (eds.). Cambridge University Press, Cambridge, United Kingdom and New York, NY, USA. 1535 pp.

Joeckel, P., Tost, H., Pozzer, A., Brühl, C., Buchholz, J., Ganzeveld, L., Hoor, P., Kerkweg, A., Lawrence, M., Sander, R., Steil, B., Stiller, G., Tanarhte, M., Taraborrelli, D., van Aardenne, J., and Lelieveld, J. The atmospheric chemistry general circulation model ECHAM5/MESSy1: consistent simulation of ozone from the surface to the mesosphere. *Atmos. Chem. Phys.*, 6:5067–2104, 2006.

Klocke, D. *Assessing the uncertainty in climate sensitivity.* PhD thesis, Universität Hamburg, Reports on Earth System Science 2011-95, Max-Planck-Institut für Meteorologie, Germany, 2011. ISSN 1614-1199.

Klocke, D., Quaas, J., and Stevens, B. Assessment of different metrics for physical climate feedbacks. *Climate Dyn.*, 41:1173–1185, 2013.

Kreyszig, E. *Statistische Methoden und ihre Anwendungen.* Vandenhoeck & Rupprecht, 1979. pp. 218.

Petty, G. W. *A first course in atmospheric radiation.* Sundog Publishing, 2006.

Ponater, M., Dietmüller, S., and Sausen, R. Greenhouse effect, radiative forcing and climate sensitivity. In Schuhmann, U., editor, *Atmospheric Physics*, pages 85–100. Springer-Verlag Berlin Heidelberg, 2012.

Roeckner, E., Bengtsson, L., Feichter, J., Lelieveld, J., and Rodhe, H. Transient Climate Change Simulations with a Coupled Atmosphere-Ocean GCM Including the Tropospheric Sulfur Cycle. *J. Climate*, 12:3004–3032, 1999.

Sausen, R., Deckert, R., Jöckel, P., Aquila, V., Brinkop, S., Burkhardt, U., Cionno, I., Dall'Amico, M., Dameris, M., Dietmüller, S., Eyring, V., Gottschaldt, K., Grewe, V., Hendricks, J., Ponater, M., and Righi, M. Global chemistry-climate modelling with EMAC. In *High Performance Computing in Science and Engineering, Garching/Munich 2009*, pages 663–674. Springer Berlin Heidelberg, 2010.

Schlesinger, M. E. *Quantitative analysis of feedbacks in climate model simulations of CO2-induced warming.* NATO ASI Series, Physically-Based Modelling and Simulation of Climate and Climatic Change, 1988.

Shell, K. M., Kiehl, J. T., and Shields, C. A. Using the Radiative Kernel Technique to Calculate Climate Feedbacks in NCAR's Community Atmospheric Model. *J. Climate*, 21:2269–2282, 2008.

Soden, B. J. and Held, I. M. An assessment of climate feedbacks in coupled ocean-atmosphere models. *J. Climate*, 19:3354–3360, 2006.

Stuber, N. *Ursachen der Variabilität des Klimasensitivitätsparameters für räumlich inhomogene Ozonstörungen.* PhD thesis, Universität Hamburg, DLR-Forschungsbericht 2003-03, Deutsches Zentrum für Luft- und Raumfahrt, Germany, 2003. ISSN 1434-8454.

Stuber, N., Ponater, M., and Sausen, R. Why radiative forcing might fail as a predictor of climate change. *Climate Dyn.*, 24:497–510, 2005.

Stuber, N., Sausen, R., and Ponater, M. Stratosphere adjusted radiative forcing calculations in a comprehensive climate model. *Theor. Appl. Climatol.*, 68:125–135, 2001.

Vial, J., Dufresne, J.-L., and Bony, S. On the interpretation of the inter-model spread in CMIP5 climate sensitivity estimates. *Climate Dyn.*, 41:3339–3362, 2013.

Wallace, J. M. and Hobbs, P. V. *Atmospheric Science - An Introductory Survey.* Elsevier, 2006. pp. 443.

Wetherald, R. T. and Manabe, S. Cloud feedback processes in a general circulation model. *J. Atmos. Sci.*, 45:1397–1415, 1988.

Wild, M., Folini, D., Schär, C., Loeb, N., Dutton, E. G., and König-Langlo, G. The global energy balance from a surface perspective. *Climate Dyn.*, 40:3107–3134, 2013.

Zdunkowski, W., Trautmann, T., and Bott, A. *Radiation in the Atmosphere - A course in Theoretical Meteorology.* Cambridge University Press, 2007. pp. 2.

Danksagung

Sehr herzlich möchte ich mich an Herrn Prof. Dr. Bernhard Mayer für die Betreuung der Arbeit und für die vielen kritischen Fragen bedanken.

Herrn Prof. Dr. Robert Sausen danke ich für die Möglichkeit meine Masterarbeit im Institut für Physik der Atmosphäre am DLR schreiben zu können.

Mein ganz besonderer Dank gilt Herrn Dr. Michael Ponater. Er ist ein ausgezeichneter Betreuer, der immer viel Zeit für Diskussionen, Erklärungen und Probleme im Programmcode hat und dies auch mal gern bei einem Kuchen oder bei einem Eis bespricht.

Für die schöne Arbeitsatmosphäre und die schönen Unterhaltungen bei den Kaffeerunden und bei den Mittagessen möchte ich mich bei der gesamten Abteilung bedanken. Insbesondere, bei meinen Mitstreitern in meinem Büro bedanke ich mich für all die leckeren Kuchen, die anregenden Diskussionen und für die Hilfe jeglicher Art!

Erklärung

Hiermit erkläre ich, die vorliegende Arbeit selbständig verfasst zu haben und keine anderen als die in der Arbeit angegebenen Quellen und Hilfsmittel benutzt zu haben.

München,